# Pulsar Tests of General Relativity

Ingrid Stairs
UBC
(on sabbatical at McGill)
Nov. 2015

Green Bank Telescope

Parkes

Arecibo

Jodrell Bank

Pulsars are neutron stars, the leftover cores of massive stars that have undergone supernova explosions.

**Masses** ~1.5 $M_\odot$
**Radii** ~10 km
**Magnetic fields** ~$10^8$ to $10^{14}$ G
**Spin rates** from ~tenths of a Hz to over 700 Hz

Not an environment that can be reproduced on Earth!

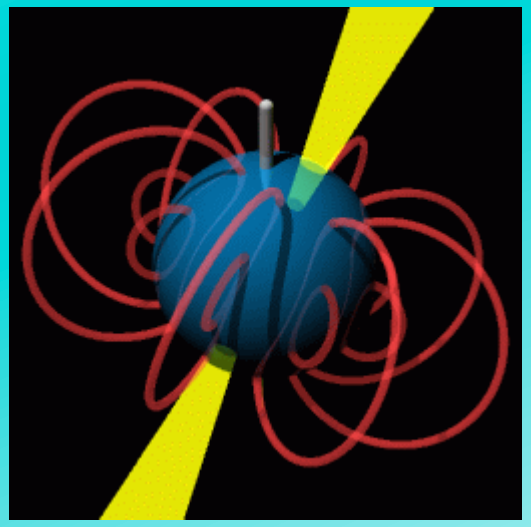

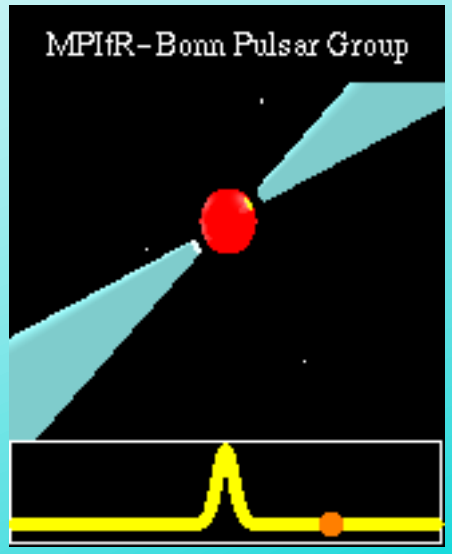


The “lighthouse” tends to have irregular beams…

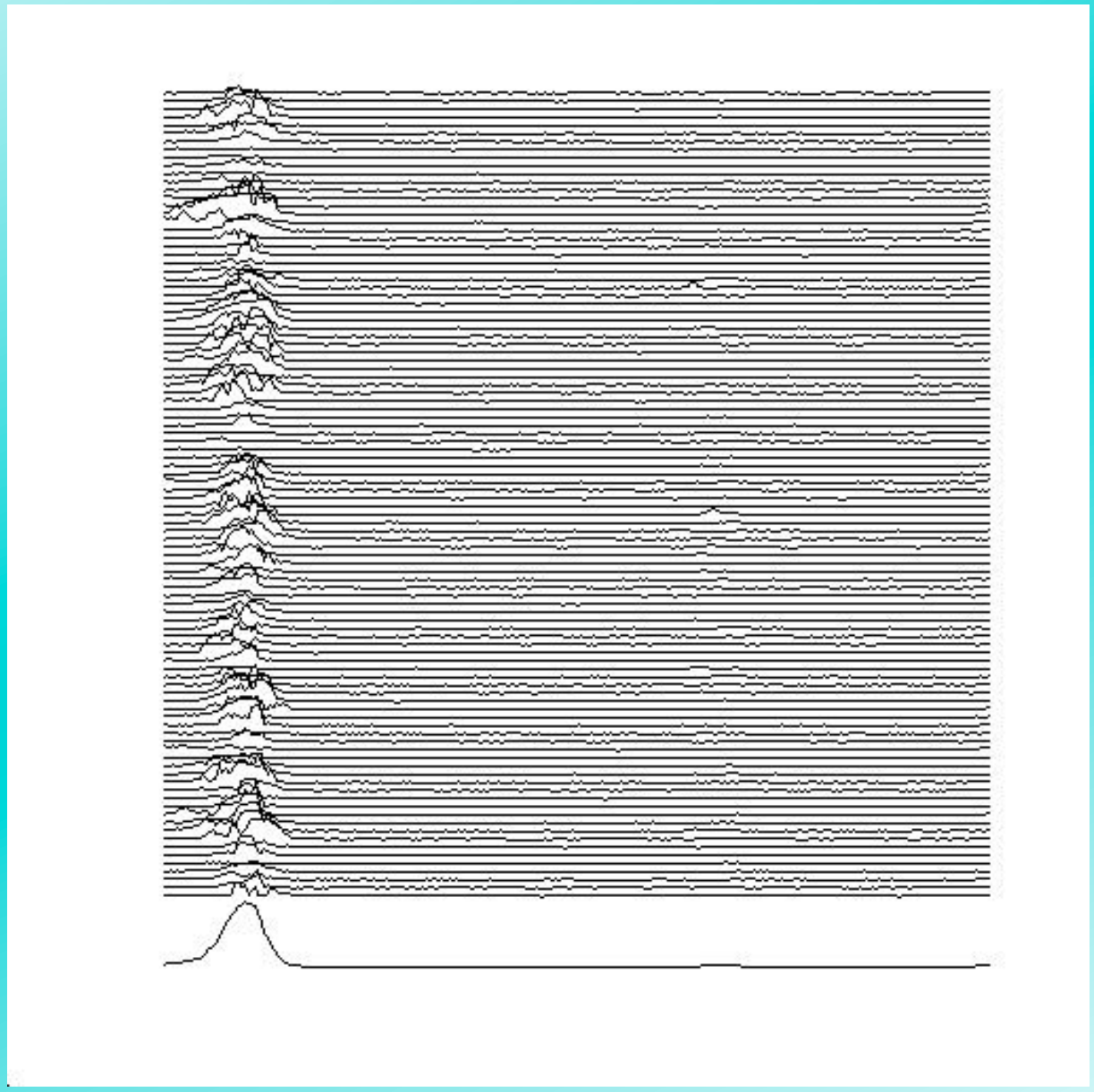

PSR B0950+08 with the Green Bank Telescope

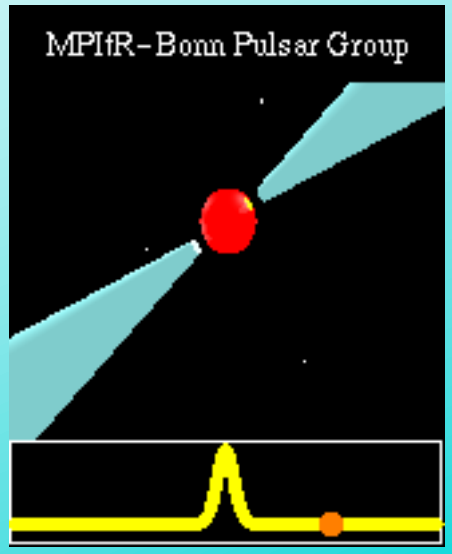


The “lighthouse” tends to have irregular beams…

…but if we add up several minutes’ worth of data, the result is a stable profile unique to each pulsar.

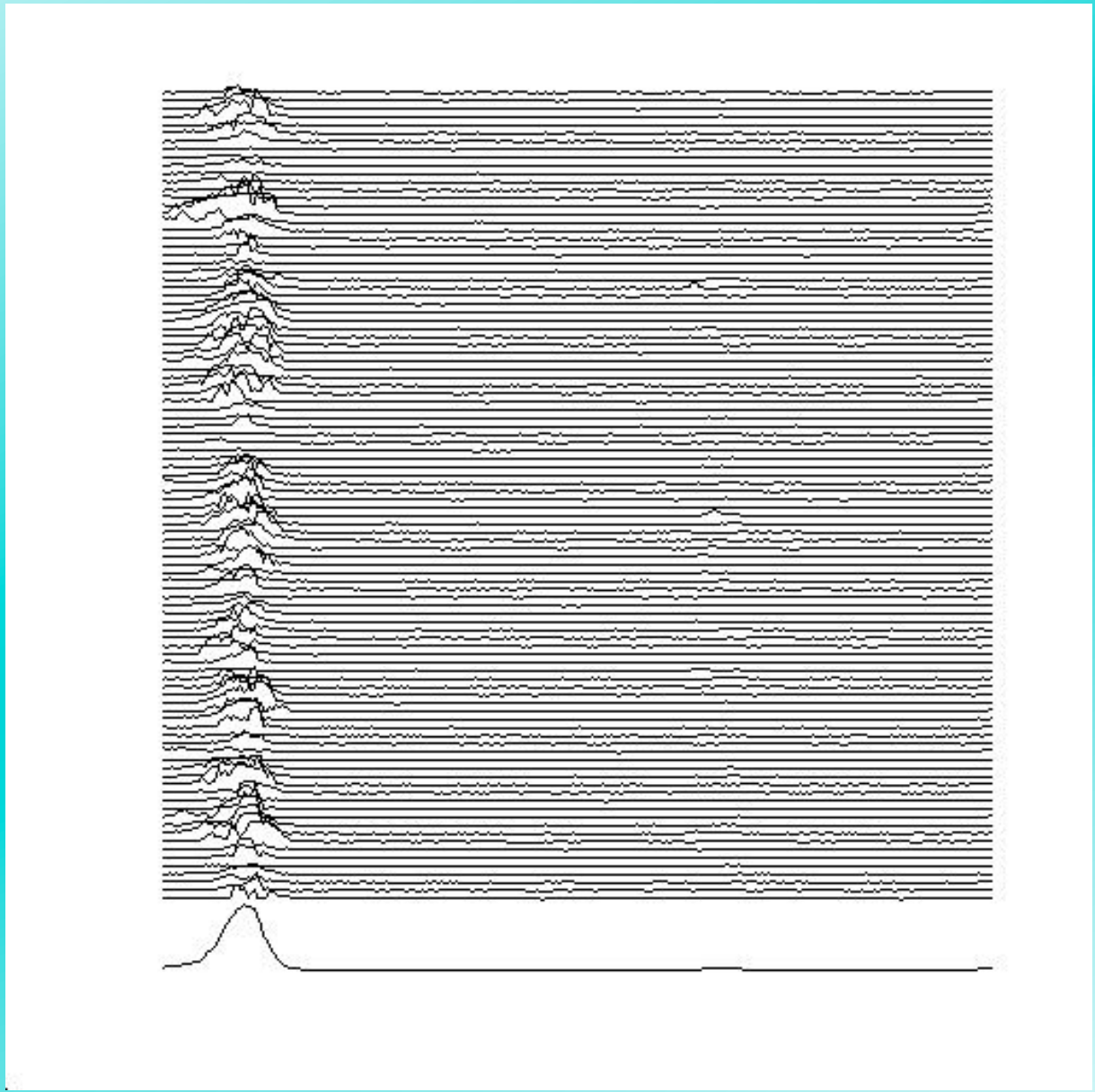

PSR B0950+08 with the Green Bank Telescope

# Pulsar Timing in a Nutshell

Standard
profile

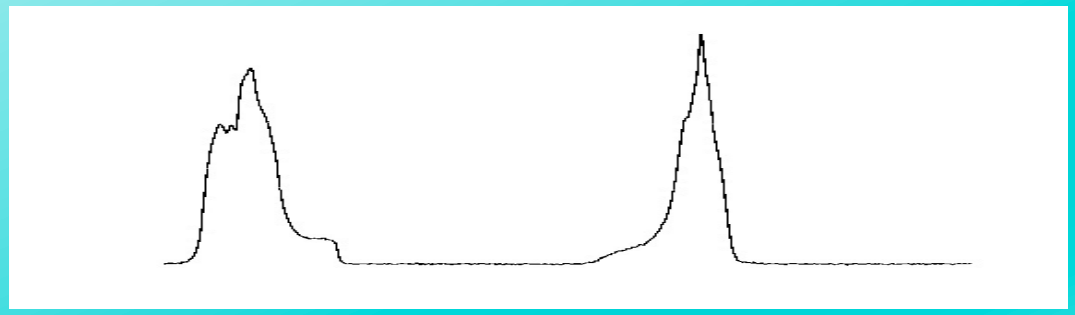

# Pulsar Timing in a Nutshell

Standard profile

Observed profile

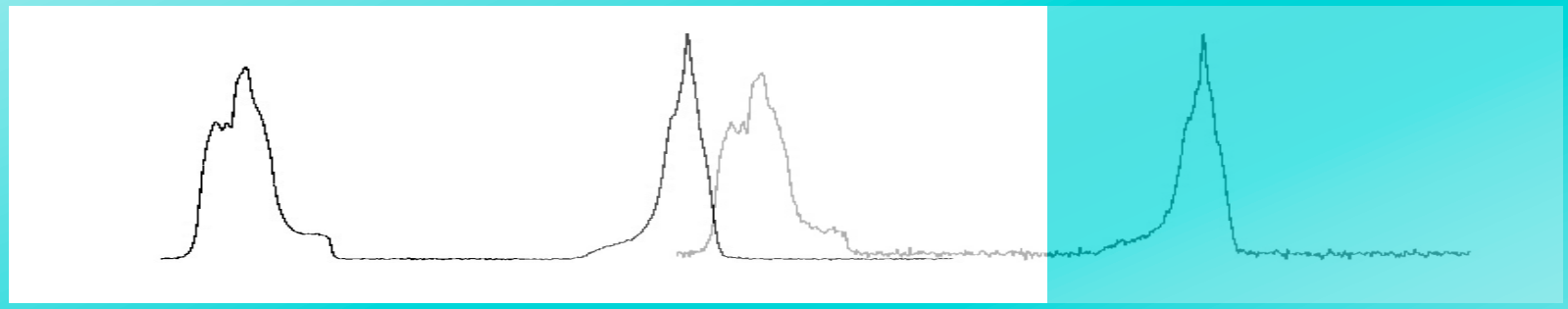

# Pulsar Timing in a Nutshell

Standard profile

Measure offset

Observed profile

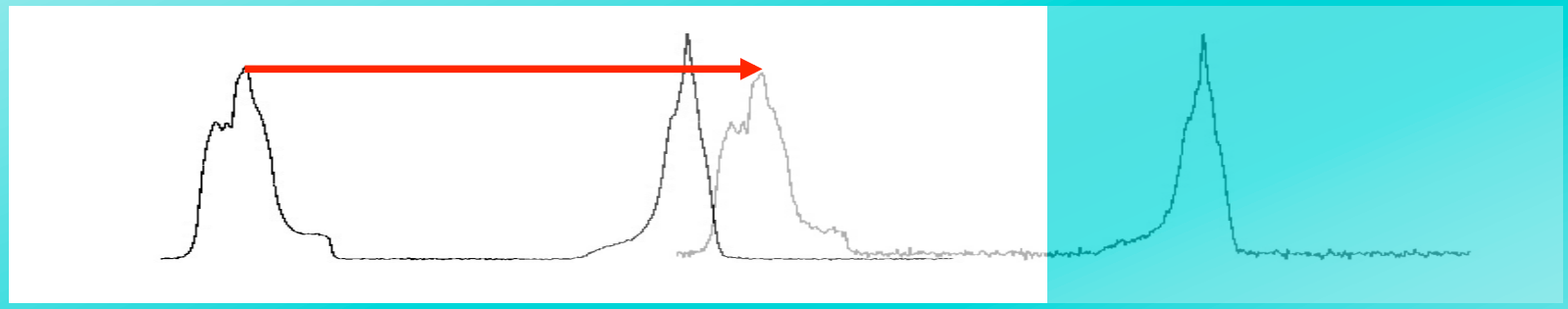

# Pulsar Timing in a Nutshell

Standard profile

Measure offset

Observed profile

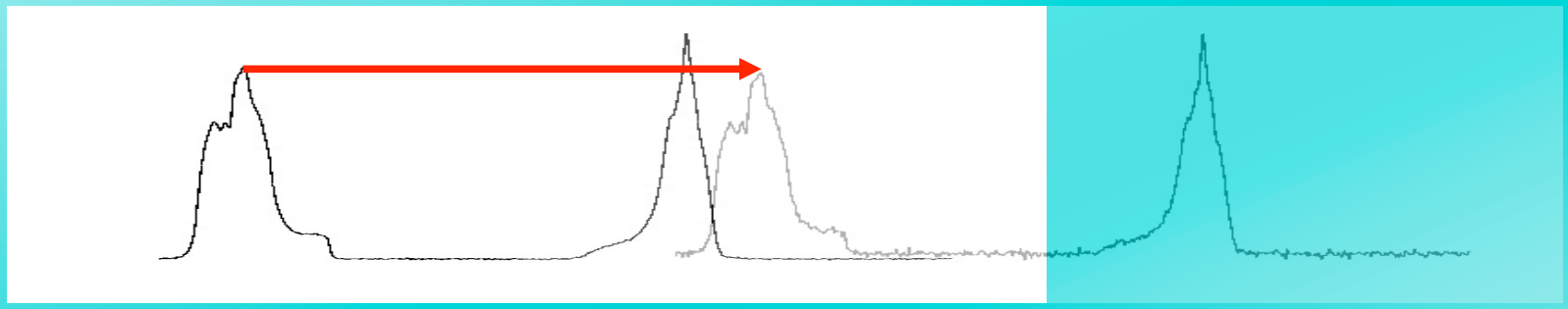

Record the start time of the observation with the observatory clock (typically a hydrogen maser).
The offset to the standard profile gives us a Time of Arrival (TOA) for the observed pulse.
Transform all TOAs to the centre of mass of the Solar System, enumerate each rotation of the pulsar and fit its parameters: spin, spin-down rate, position, binary parameters...

# Timing Residuals: Actual pulse Times of Arrival (TOAs) – Predicted TOAs

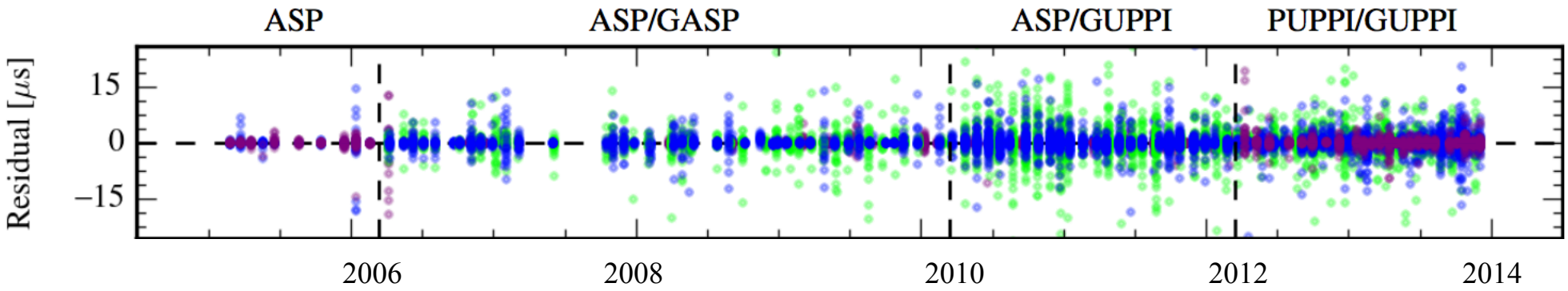


PSR J1713+0747 – Arzoumanian et al., ApJ, **813**, 65 (2015) (NANOGrav 9-year data release)

Gaussian residuals imply a good ephemeris (spin, astrometry, binary parameters...).

# Pulsars available for GR tests

Young pulsars

Recycled pulsars

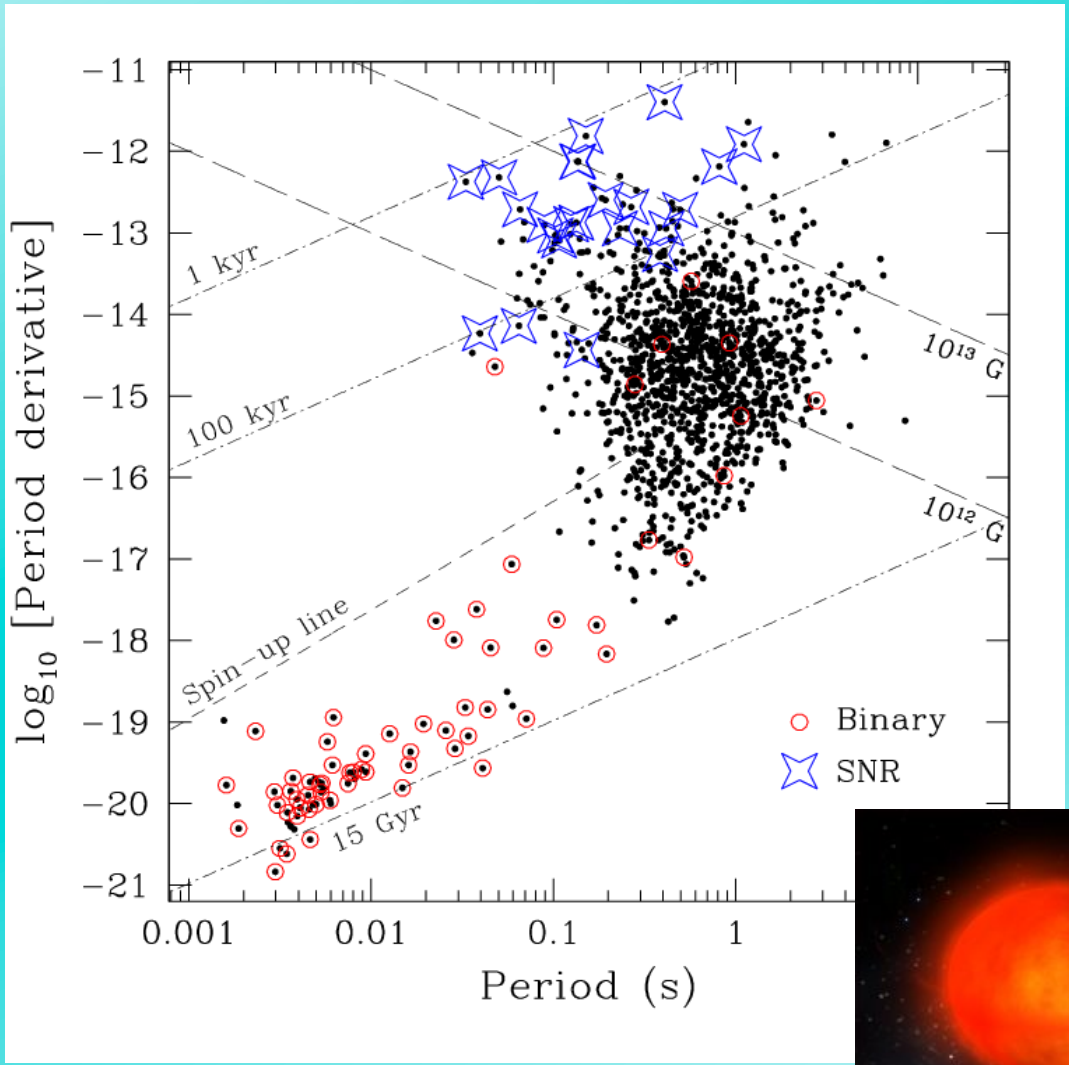


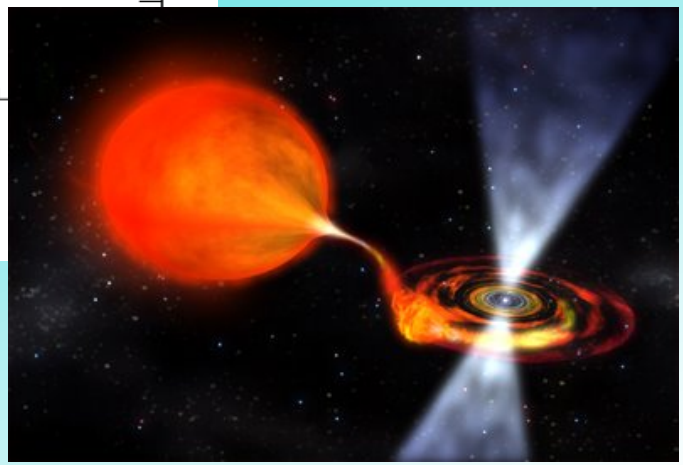

NASA/Dana Berry

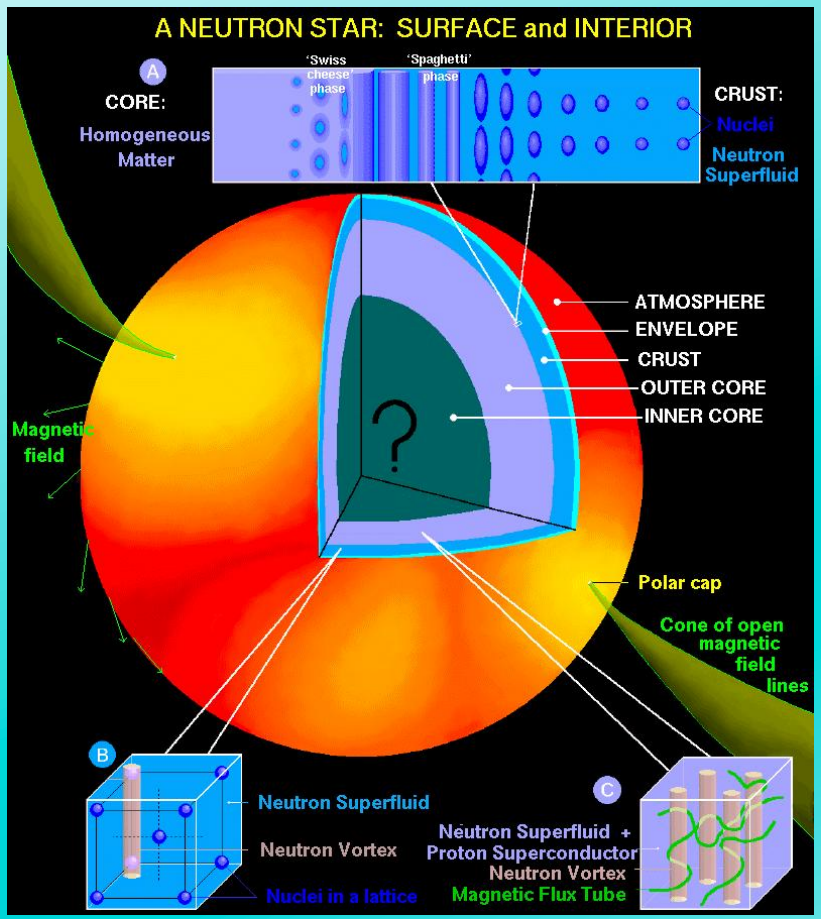


D. Page

**Why use pulsars to test theories of gravity?** Some alternative theories behave like General Relativity in the weak gravitational field of the Solar System, but very differently near compact objects. The coupling to the extra parameters in these theories might depend on the structure and gravitational binding energy of the compact objects.

**Gravitational binding energy comparison:**

White dwarfs (WD): 0.01% of mass
Neutron stars (NS): 10--20% of mass
Black holes (BH): 50% of mass

# Equivalence Principle Violations

Pulsar timing can:

- set limits on several of the Parametrized Post-Newtonian (PPN) parameters
- test for violations of the Strong Equivalence Principle (SEP) through
  - the Nordtvedt Effect
  - dipolar gravitational radiation
  - variations of Newton's constant

(Actually, parameters modified to account for compactness of neutron stars.)

(Damour & Esposito-Farèse 1992, CQG, 9, 2093; 1996, PRD, 53, 5541).

# SEP: Nordtvedt (Gravitational Stark) Effect

Lunar Laser Ranging: Moon's orbit is not polarized toward Sun.

$$\eta = 4\beta - \gamma - 3 - \frac{10}{3}\xi - \alpha_1 + \frac{2}{3}\alpha_2 - \frac{2}{3}\zeta_1 - \frac{1}{3}\zeta_2$$

Constraint: $\eta = (-1.7 \pm 2.9) \times 10^{-4}$
(Williams et al. 2012, CGQ **29**, 184004)

WD NS

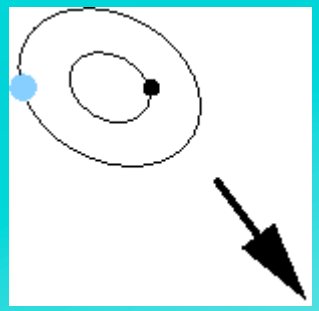

Result is a polarized orbit.

Binary pulsars: NS and WD fall differently in gravitational field of Galaxy.

$$\left(\frac{m^{\text{grav}}}{m^{\text{inertial}}}\right) = 1 + \Delta_i$$

$$= 1 + \eta\left(\frac{E^{\text{grav}}}{m_i}\right) + \eta'\left(\frac{E^{\text{grav}}}{m_i}\right)^2 + \ldots$$

Constrain $\Delta_{\text{net}} = \Delta_{\text{NS}} - \Delta_{\text{WD}}$

(Damour & Schäfer 1991, PRL, 66, 2549.)

# Deriving a Constraint on $\Delta_{net}$

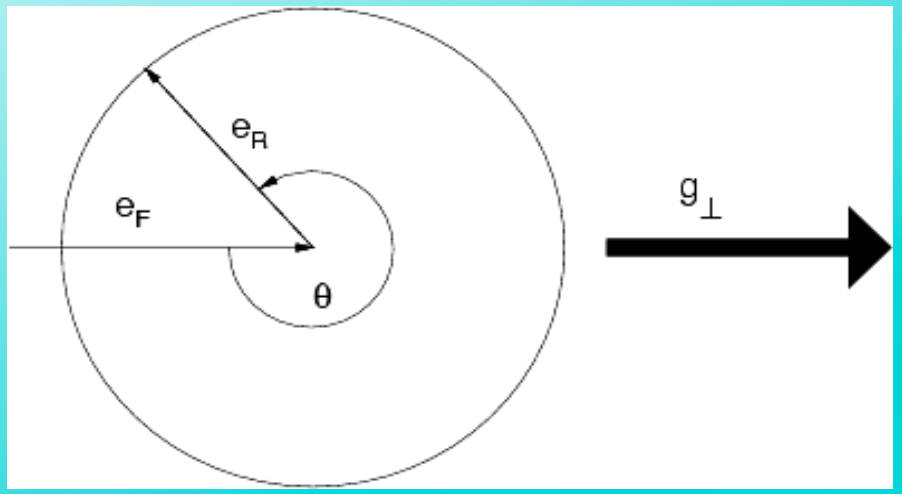


After Wex 1997, A&A, 317, 976.

Use pulsar—white-dwarf binaries with low eccentricities ( $<10^{-3}$).
Eccentricity would contain a "forced" component along projection of Galactic gravitational force onto the orbit. This may partially cancel "natural" eccentricity.

Constraint $\propto P_b^2/e$. Need to estimate orbital inclination and masses.
Formerly: assume binary orbit is randomly oriented on sky.
Use all similar systems to counter selection effects (Wex).
Ensemble of pulsars: $\Delta_{net} < 9 \times 10^{-3}$ (Wex 1997, A&A, 317, 976; 2000, ASP Conf. Ser.).

More recently: use information about longitude of periastron (previously unused) and measured eccentricity and a Bayesian formulation to construct pdfs for $\Delta_{net}$ for each appropriate pulsar, representing the full population of similar objects.

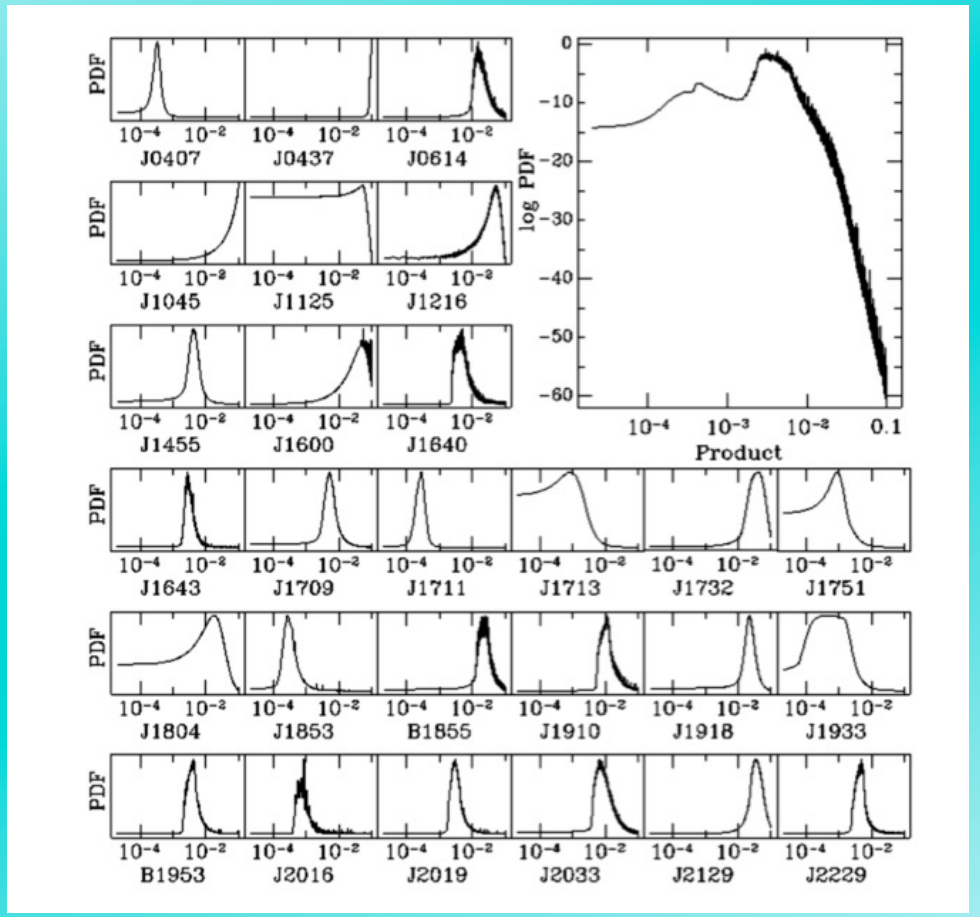


Gonzalez et al. 2011

Result: $|\Delta_{net}| < 0.0046$ at 95% confidence (Gonzalez et al. 2011, ApJ, **743**, 102, based on method used in Stairs et al. 2005).

Another plan: try to measure e-dot in wide-orbit pulsar/WD binaries (Freire et al. 2012, CQG **29**, 400) – any e-dot induced by a non-zero $\Delta$ should be several orders of magnitude larger than that expected from gravitational radiation or aberration. A detection of e-dot would represent an actual detection of $\Delta$, not just an upper limit.

Arguably even better would be a detection of e-dot in a system with large eccentricity, such as the millisecond pulsar--main-sequence binary J1903+0327. This particular pulsar is quite massive ($1.667 \pm 0.021\ M_\odot$) and might therefore have stronger coupling to a non-GR field, eg through spontaneous scalarization.

A new prospect for SEP tests! The triple system J0337+1715 (Ransom et al. 2014, Nature **505**, 520),

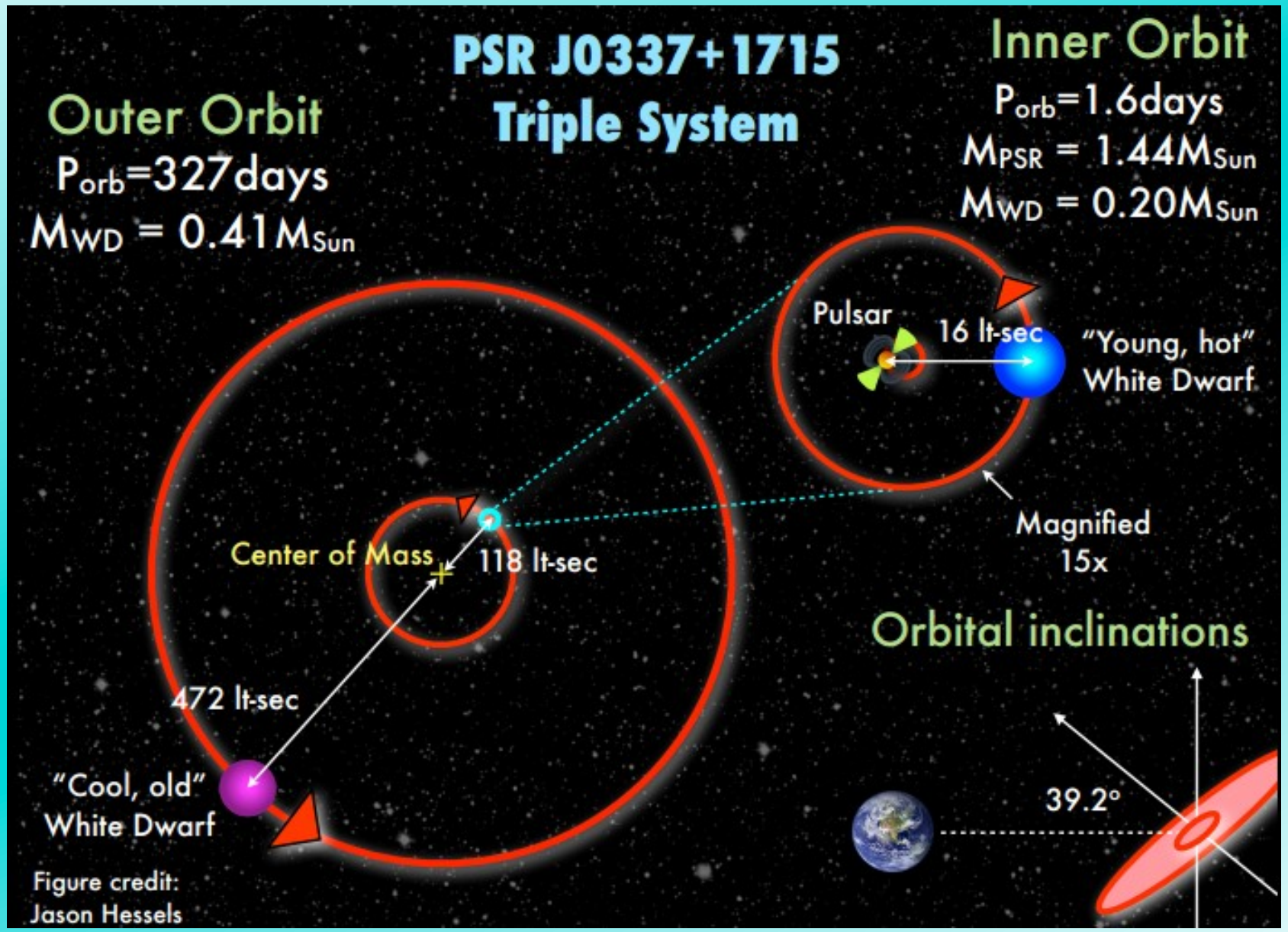

Long-term timing observations with Arecibo, Green Bank and Westerbork.

Eventually, Anne Archibald (ASTRON) was able to develop a full model of the system ephemeris using numerical integration and MCMC parameter estimation (bottom panel).

So far, the solution has only required Newtonian orbits plus second-order Doppler shift, time dilation due to depth in the gravitational fields and Shapiro delay – not a fully relativistic model.

Ransom et al 2014

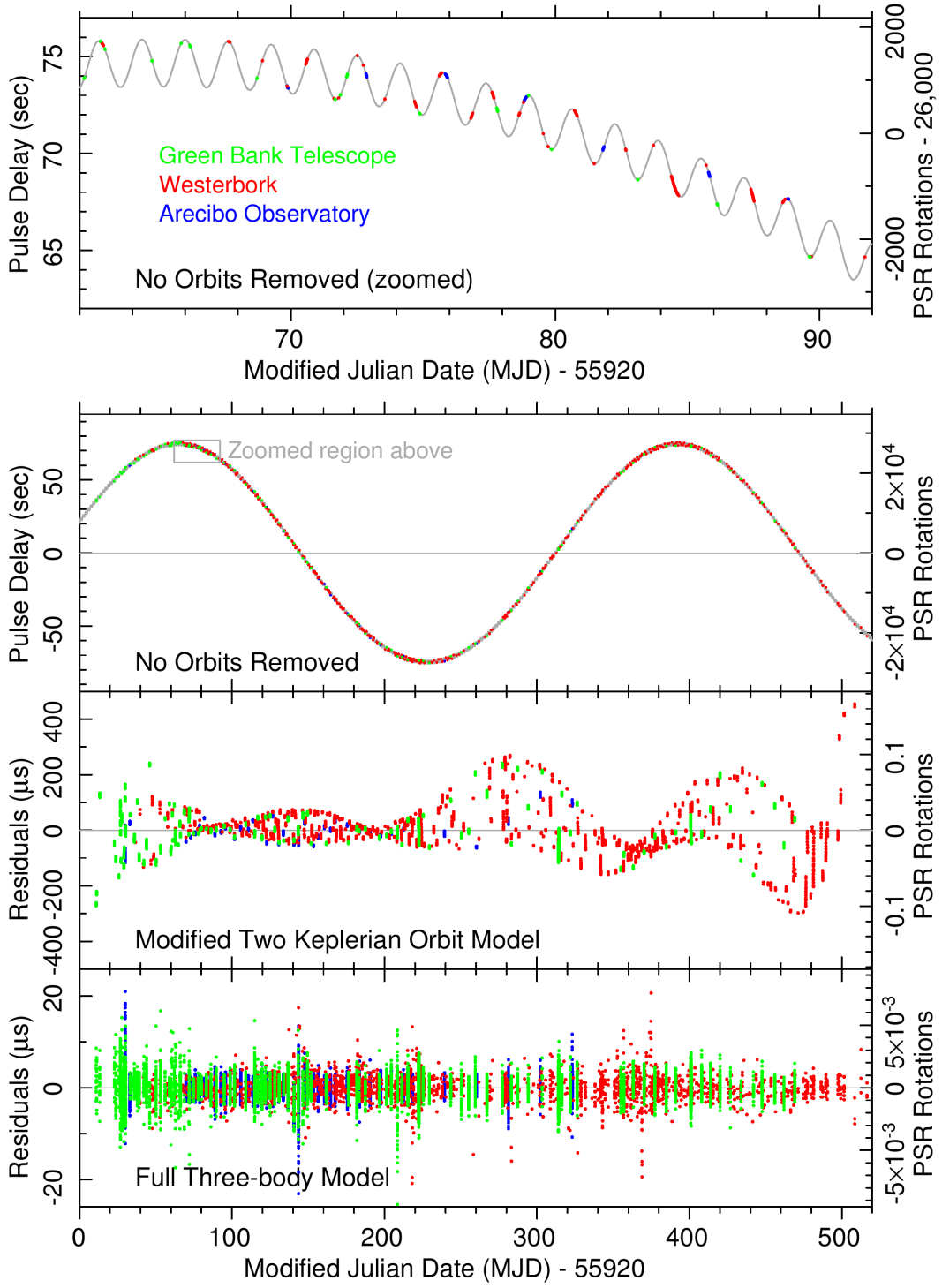

Features of the timing solution:
a) the longitudes of periastron (apsides) of the orbits are nearly aligned, but librate – expected;
b) the orbits are nearly coplanar and nearly circular – not so expected.

| Parameter | Symbol | Value |
|---|---|---|
| **Fixed values** | | |
| Right ascension | RA | $03^h37^m43^s.82589(13)$ |
| Declination | Dec | $17°15'14''.828(2)$ |
| Dispersion measure | DM | $21.3162(3)$ pc cm$^{-3}$ |
| Solar system ephemeris | | DE405 |
| Reference epoch | | MJD 55920.0 |
| Observation span | | MJD $55930.9 - 56436.5$ |
| Number of TOAs | | 26280 |
| Weighted root-mean-squared residual | | $1.34\,\mu$s |
| **Fitted parameters** | | |
| **Spin-down parameters** | | |
| Pulsar spin frequency | $f$ | $365.953363096(11)$ Hz |
| Spin frequency derivative | $\dot{f}$ | $-2.3658(12) \times 10^{-15}$ Hz s$^{-1}$ |
| **Inner Keplerian parameters for pulsar orbit** | | |
| Semimajor axis projected along line of sight | $(a \sin i)_I$ | 1.21752844(4) lt-s |
| Orbital period | $P_{b,I}$ | 1.629401788(5) d |
| Eccentricity parameter $(e \sin \omega)_I$ | $\epsilon_{1,I}$ | $6.8567(2) \times 10^{-4}$ |
| Eccentricity parameter $(e \cos \omega)_I$ | $\epsilon_{2,I}$ | $-9.171(2) \times 10^{-5}$ |
| Time of ascending node | $t_{\mathrm{asc},I}$ | MJD 55920.407717436(17) |
| **Outer Keplerian parameters for centre of mass of inner binary** | | |
| Semimajor axis projected along line of sight | $(a \sin i)_O$ | 74.6727101(8) lt-s |
| Orbital period | $P_{b,O}$ | 327.257541(7) d |
| Eccentricity parameter $(e \sin \omega)_O$ | $\epsilon_{1,O}$ | $3.5186279(3) \times 10^{-2}$ |
| Eccentricity parameter $(e \cos \omega)_O$ | $\epsilon_{2,O}$ | $-3.462131(11) \times 10^{-3}$ |
| Time of ascending node | $t_{\mathrm{asc},O}$ | MJD 56233.935815(7) |
| **Interaction parameters** | | |
| Semimajor axis projected in plane of sky | $(a \cos i)_I$ | 1.4900(5) lt-s |
| Semimajor axis projected in plane of sky | $(a \cos i)_O$ | 91.42(4) lt-s |
| Inner companion mass over pulsar mass | $q_I = m_{cI}/m_p$ | 0.13737(4) |
| Difference in longs. of asc. nodes | $\delta_\Omega$ | $2.7(6) \times 10^{-3}$ ° |
| **Inferred or derived values** | | |
| **Pulsar properties** | | |
| Pulsar period | $P$ | 2.73258863244(9) ms |
| Pulsar period derivative | $\dot{P}$ | $1.7666(9) \times 10^{-20}$ |
| Inferred surface dipole magnetic field | $B$ | $2.2 \times 10^8$ G |
| Spin-down power | $\dot{E}$ | $3.4 \times 10^{34}$ erg s$^{-1}$ |
| Characteristic age | $\tau$ | $2.5 \times 10^9$ y |
| **Orbital geometry** | | |
| Pulsar semimajor axis (inner) | $a_I$ | 1.9242(4) lt-s |
| Eccentricity (inner) | $e_I$ | $6.9178(2) \times 10^{-4}$ |
| Longitude of periastron (inner) | $\omega_I$ | 97.6182(19) ° |
| Pulsar semimajor axis (outer) | $a_O$ | 118.04(3) lt-s |
| Eccentricity (outer) | $e_O$ | $3.53561955(17) \times 10^{-2}$ |
| Longitude of periastron (outer) | $\omega_O$ | 95.619493(19) ° |
| Inclination of invariant plane | $i$ | 39.243(11) ° |
| Inclination of inner orbit | $i_I$ | 39.254(10) ° |
| Angle between orbital planes | $\delta_i$ | $1.20(17) \times 10^{-2}$ ° |
| Angle between eccentricity vectors | $\delta_\omega \sim \omega_O - \omega_I$ | $-1.9987(19)$ ° |
| **Masses** | | |
| Pulsar mass | $m_p$ | 1.4378(13) $M_\odot$ |
| Inner companion mass | $m_{cI}$ | 0.19751(15) $M_\odot$ |
| Outer companion mass | $m_{cO}$ | 0.4101(3) $M_\odot$ |

The system geometry, along with some helpful length scales for reference. The coplanarity, circularity and very hierarchical nature of the orbits imply long-term stability, making it “easier” to find such a triple.

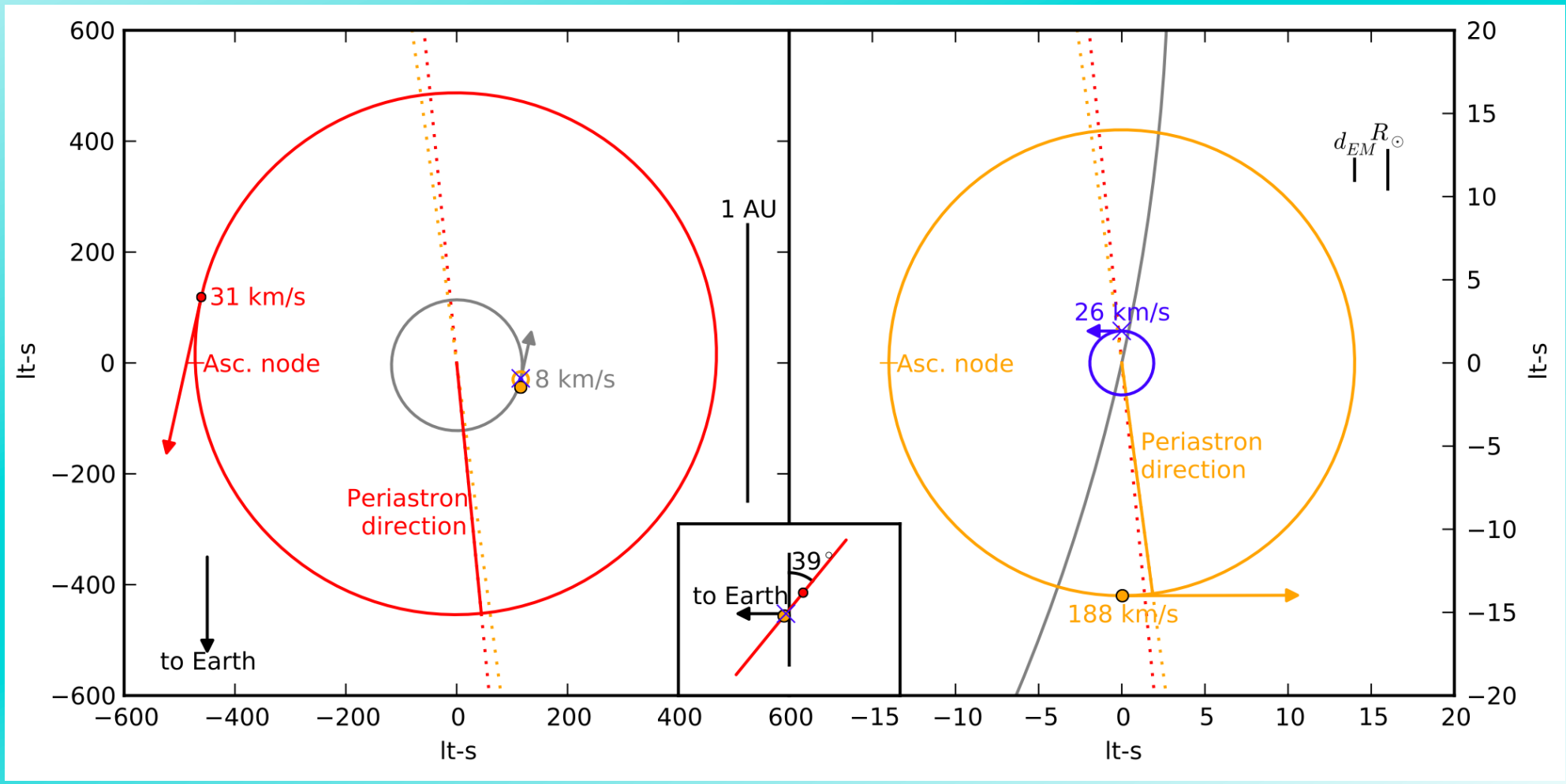


Ransom et al 2014

# Testing the SEP with PSR J0337+1715

We will do a test that is much more like the Lunar Laser Ranging test: If $\Delta$ is non-zero, we would expect the pulsar and the inner WD to fall differently in the gravitational field of the outer WD – in other words, the eccentricity vector of the inner orbit should contain a component that tracks the position of the outer WD. This gravitational field is about $10^6$ times stronger than that of the Galaxy, so the test should be correspondingly more stringent.

In practice, the test is being set up so that the gravitational and inertial masses of the pulsar are fit as two separate parameters in a relativistic timing solution that allows for the PPN parameters.

We expect to achieve a constraint on $\Delta$ of order $5 \times 10^{-7}$, or on $\eta$ of order $5 \times 10^{-6}$. This will be much better than the Solar Systems tests of $\eta$ and will also test for the violation in the strong-field regime of gravity.

# Constraints on $\alpha_1$ and $\alpha_3$

$\alpha_1$: Implies existence of preferred frames.
Expect orbit to be polarized along projection of velocity (wrt CMB) onto orbital plane. Constraint $\propto P_b^{1/3}/e$.

Ensemble of pulsars: $\alpha_1 < 1.4 \times 10^{-4}$ (Wex 2000, ASP Conf. Ser.).

Comparable to LLR tests (Müller et al. 1996, PRD, 54, R5927).

This test now needs updating with Bayesian approach...

$\alpha_3$: Violates local Lorentz invariance and conservation of momentum. Expect orbit to be polarized, depending on cross-product of system velocity and pulsar spin. Constraint $\propto P_b^2/(eP)$, same pulsars used as for $\Delta$ test.

Ensemble of pulsars: $\alpha_3 < 5.5 \times 10^{-20}$ (Gonzalez et al. 2011; slightly worse limit than in Stairs et al. 2005, ApJ, 632, 1060, but more information used).

(Cf. Perihelion shifts of Earth and Mercury: $\sim 2 \times 10^{-7}$ (Will 1993, "Theory & Expt. In Grav. Physics," CUP))

## New Methods to Constrain $\alpha_1$, $\alpha_2$ and $\xi$– Shao & Wex 2012, CQG **29**, 215018; Shao et al. 2013, Marcel Grossman Proceedings, , Shao et al. 2013, CQG 30 165019, Shao & Wex 2013, CQG **30** 165020.

For $\alpha_1$, still use short-period PSR-WD binaries, but look for changes in the eccentricity vector, recognizing that periastron precession will eventually reveal the "forced" component of the eccentricity. Limit from PSR J1738+0333: $\alpha_1 = -0.4^{+3.7}_{-3.1} \times 10^{-5}$.

For $\alpha_2$, look for an apparent time derivative of the projected semi-major axis in short-orbital period PSR-WD systems, indicating precession of the orbital plane about the velocity vector relative to the preferred frame. Limit from PSRs J1012+5307 and J1738+0333: $|\alpha_2| < 1.8 \times 10^{-4}$. Limit from MSP profile stability: $|\alpha_2| < 1.6 \times 10^{-9}$.

A similar argument is used for $\xi$, with the relevant vector being that of the Galactic gravitational vector. Limit: $|\xi| < 3.1 \times 10^{-4}$. Can also argue from the stability of MSP profiles: $|\xi| < 3.9 \times 10^{-9}$.

# Orbital Decay Tests

These rely on measurement of or constraint on orbital period derivative, $\dot{P}_b$ .
This is complicated by systematic biases:

$$\left(\frac{\dot{P}_b}{P_b}\right)_{\text{Observed}} = \left(\frac{\dot{P}_b}{P_b}\right)_{\text{Accel}} + \cancel{\left(\frac{\dot{P}_b}{P_b}\right)_{\dot{G}}} + \cancel{\left(\frac{\dot{P}_b}{P_b}\right)_{\dot{m}}} + \left(\frac{\dot{P}_b}{P_b}\right)_{\text{Quadrupolar}} + \left(\frac{\dot{P}_b}{P_b}\right)_{\text{Dipolar}}$$

$$\left(\frac{\dot{P}_b}{P_b}\right)_{\text{Accel}} = \left(\frac{\dot{P}_b}{P_b}\right)_{\text{gravitational field}} + \left(\frac{\dot{P}_b}{P_b}\right)_{\text{Shklovskii}}$$

$$\left(\frac{\dot{P}_b}{P_b}\right)_{\text{Shklovskii}} = \mu^2 \frac{d}{c}$$

# Dipolar Gravitational Radiation

Difference in gravitational binding energies of NS and WD implies dipolar gravitational radiation possible in, e.g., tensor-scalar theories.

$$\dot{P}_{b\,\mathrm{Dipole}} = \frac{4\pi^2 G_*}{c^3 P_b}\frac{m_1 m_2}{m_1 + m_2}\left(\alpha_{c_1} - \alpha_{c_2}\right)^2$$

Damour & Esposito-Farèse 1996, PRD, 54, 1474.

Test using pulsar—WD systems in short-period orbits. The best test at this time is given by:

PSR J1738+0333, 8.5-hour orbit:

$\left(\alpha_{cp} - \alpha_0\right)^2 < (1.8\pm3.6)\times10^{-6}$ (Freire et al. 2012, MNRAS **433**, 3328)

Note that we also have a limit of $2.5 \times 10^{-5}$ for the 2-$M_\odot$ pulsar PSR J0348+0438 (2.5-hour orbit, Antoniadis et al. 2013, Science, **340**, 448) – this will be important when considering mass-dependent deviations from GR.

Orbital decay tests rely on measurement of or constraint on orbital period derivative, $\dot{P}_b$ .

This is complicated by systematic biases:

$$\left(\frac{\dot{P}_b}{P_b}\right)_{\text{Observed}} = \left(\frac{\dot{P}_b}{P_b}\right)_{\text{Accel}} + \left(\frac{\dot{P}_b}{P_b}\right)_{\dot{G}} + \left(\frac{\dot{P}_b}{P_b}\right)_{\dot{m}} + \left(\frac{\dot{P}_b}{P_b}\right)_{\text{Quadrupolar}} + \left(\frac{\dot{P}_b}{P_b}\right)_{\text{Dipolar}}$$

$$\left(\frac{\dot{P}_b}{P_b}\right)_{\text{Accel}} = \left(\frac{\dot{P}_b}{P_b}\right)_{\text{gravitational field}} + \left(\frac{\dot{P}_b}{P_b}\right)_{\text{Shklovskii}}$$

$$\left(\frac{\dot{P}_b}{P_b}\right)_{\text{Shklovskii}} = \mu^2 \frac{d}{c}$$

# Variation of Newton's Constant

Spin: Variable G changes moment of inertia of NS.

Expect $\frac{\dot{P}}{P} \propto \frac{\dot{G}}{G}$ depending on equation of state, PM correction...

Various millisecond pulsars, roughly: $\frac{\dot{G}}{G} \leq 2 \times 10^{-11}\,\mathrm{yr}^{-1}$

Orbital decay: Expect $\frac{\dot{P}_b}{P_b} \propto \frac{\dot{G}}{G}$, test with circular NS-WD binaries.

PSR B1855+09, 12.3-day orbit: $\frac{\dot{G}}{G} = (-1.3 \pm 2.7) \times 10^{-11}\,\mathrm{yr}^{-1}$

(Kaspi, Taylor & Ryba 1994, ApJ, **428**, 713; Arzoumanian 1995, PhD thesis, Princeton).

PSR J0437-4715, 5.7-day orbit: $\frac{\dot{G}}{G} = (0.5 \pm 2.6) \times 10^{-12}\,\mathrm{yr}^{-1}$

(Verbiest et al 2008, ApJ **679**, 675, 95% confidence, using slightly different assumptions).

PSR J1713+0747, 67.8-day orbit: $\frac{\dot{G}}{G} = (-0.6 \pm 1.1) \times 10^{-12}\,\mathrm{yr}^{-1}$

(Zhu et al 2015, ApJ, **809**, 41).

Not as constraining as LLR (Hoffman et al. 2010, A&A, **522**, L5: $\frac{\dot{G}}{G} = (-0.7 \pm 7.6) \times 10^{-13}\,\mathrm{yr}^{-1}$

# Combined Limit on $\dot{G}$ and Dipolar Gravitational Radiation

Lazaridis et al. 2009 (MNRAS 400, 805) combine the $\dot{P}_b$ limits from J1012+5307 and J0437-4715 to form a combined limit on these two quantities:

$$\frac{\dot{G}}{G} = (-0.7 \pm 3.3) \times 10^{-12}\,\mathrm{yr}^{-1}$$

and $$\kappa_D \approx \frac{(\alpha_{cp} - \alpha_0)^2}{S^2} = (0.3 \pm 2.5) \times 10^{-3}$$

Best current limit uses J1012+5307, J1738+0333 and J1713+0747 (Zhu et al 2015):

$$\frac{\dot{G}}{G} = (0.6 \pm 1.1) \times 10^{-12}\,\mathrm{yr}^{-1}$$

and $$\kappa_D \approx \frac{(\alpha_{cp} - \alpha_0)^2}{S^2} = (-0.9 \pm 3.3) \times 10^{-4}$$

# Relativistic Binaries

Binary pulsars, especially double-neutron-star systems: measure post-Keplerian (PK) **timing** parameters in a theory-independent way (Damour & Deruelle 1986, AIHP, 44, 263). These predict the stellar masses in any theory of gravity. In GR, to 1st Post-Newtonian (PN) order:

$$\dot{\omega} = 3\left(\frac{P_b}{2\pi}\right)^{-5/3}\left(T_0 M\right)^{2/3}\left(1-e^2\right)^{-1}$$

$$\gamma = e\left(\frac{P_b}{2\pi}\right)^{1/3} T_0^{\,2/3} M^{-4/3} m_2\left(m_1+2m_2\right)$$

$$\dot{P}_b = \frac{-192}{5}\left(\frac{P_b}{2\pi}\right)^{-5/3}\left(1+\frac{73}{24}e^2+\frac{37}{96}e^4\right)\left(1-e^2\right)^{-7/2} T_0^{\,5/3} m_1 m_2 M^{-1/3}$$

$$r = T_0 m_2$$

$$s = x\left(\frac{P_b}{2\pi}\right)^{-2/3} T_0^{\,-1/3} M^{-2/3} m_2^{\,-1}$$

$$M = m_1 + m_2$$

$$T_0 = 4.925490947\,\mu s$$

# The Original System: PSR B1913+16

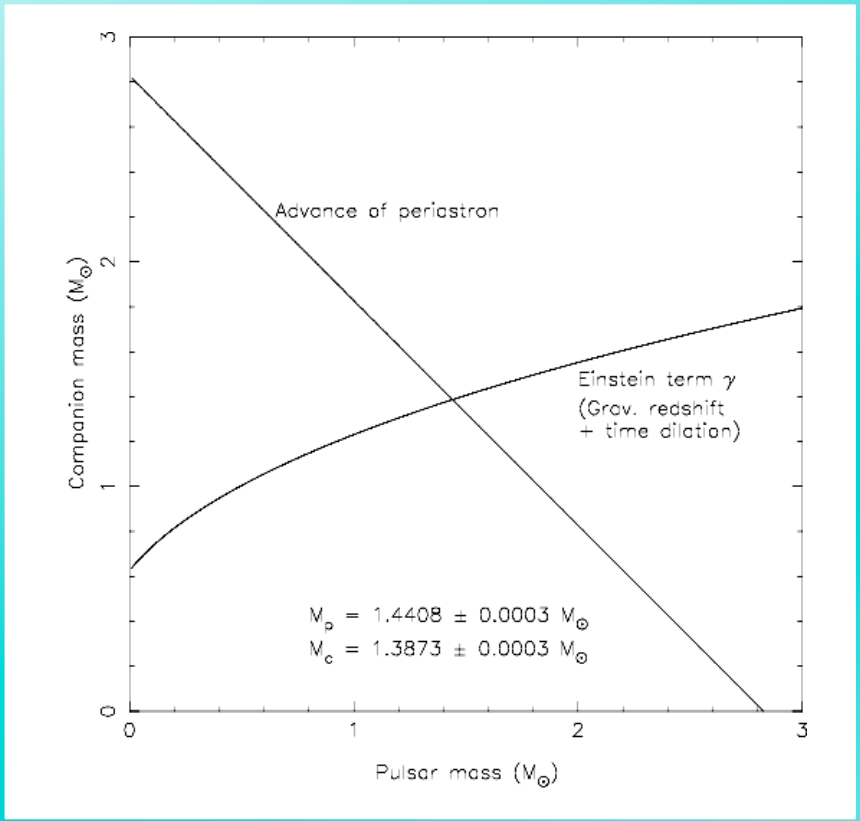


Highly eccentric double-NS system, 8-hour orbit.

The $\dot{\omega}$ and γ parameters predict the pulsar and companion masses.

The $\dot{P}_b$ parameter is in good agreement, to ~0.2%. Galactic acceleration modeling now limits this test.

Weisberg & Taylor 2003, ASP Conf. Ser. 302, 93
(Courtesy Joel Weisberg)

# Orbital Decay of PSR B1913+16

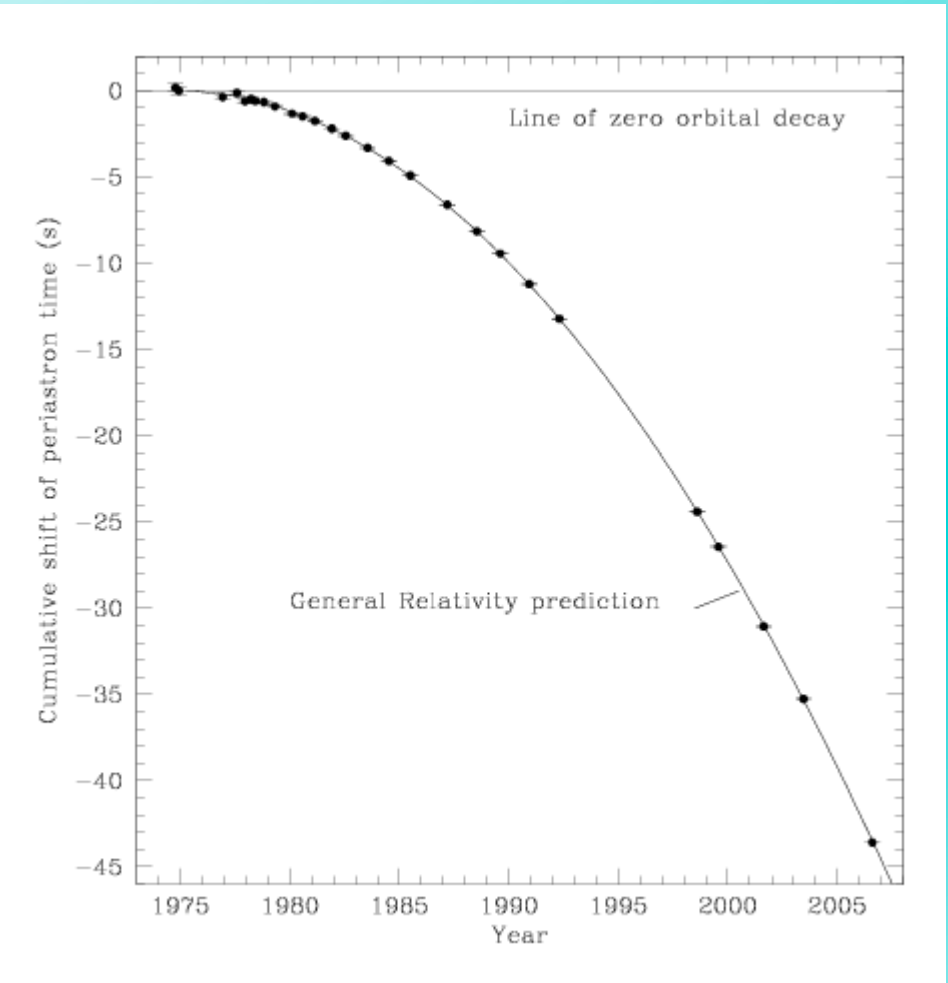


The accumulated shift of periastron passage time, caused by the decay of the orbit.
A good match to the predictions of GR!

Weisberg, Nice & Taylor, 2010, ApJ **722**, 1030

# PSR B1534+12 – Fonseca, Stairs & Thorsett 2014, ApJ **787** 82.

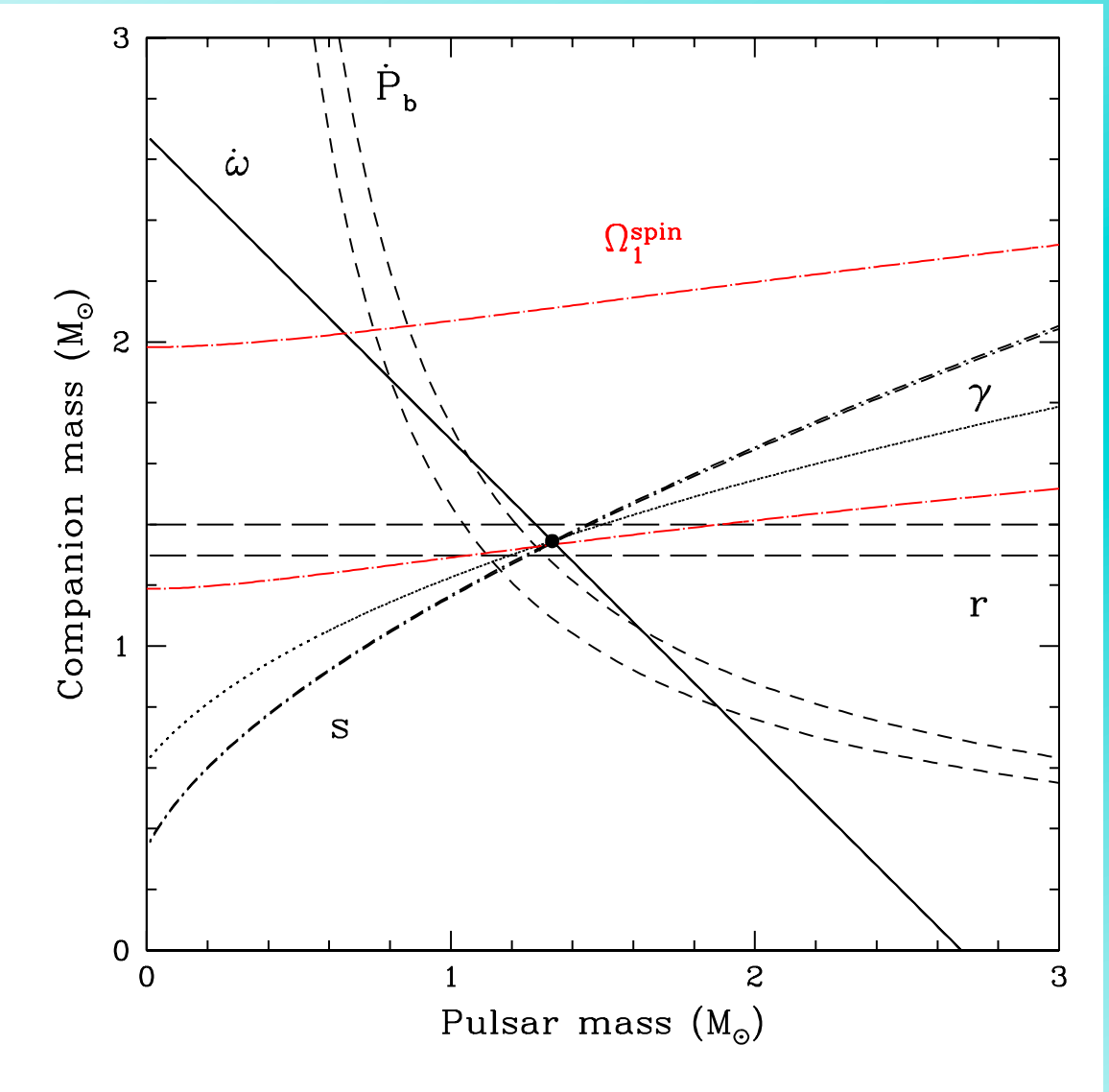


Pulsar mass is 1.3330(2) $M_\odot$. Companion mass is 1.3455(2) $M_\odot$.

Best estimate of distance, based on assumption of GR-derived orbital decay, is 1.051(5) kpc.

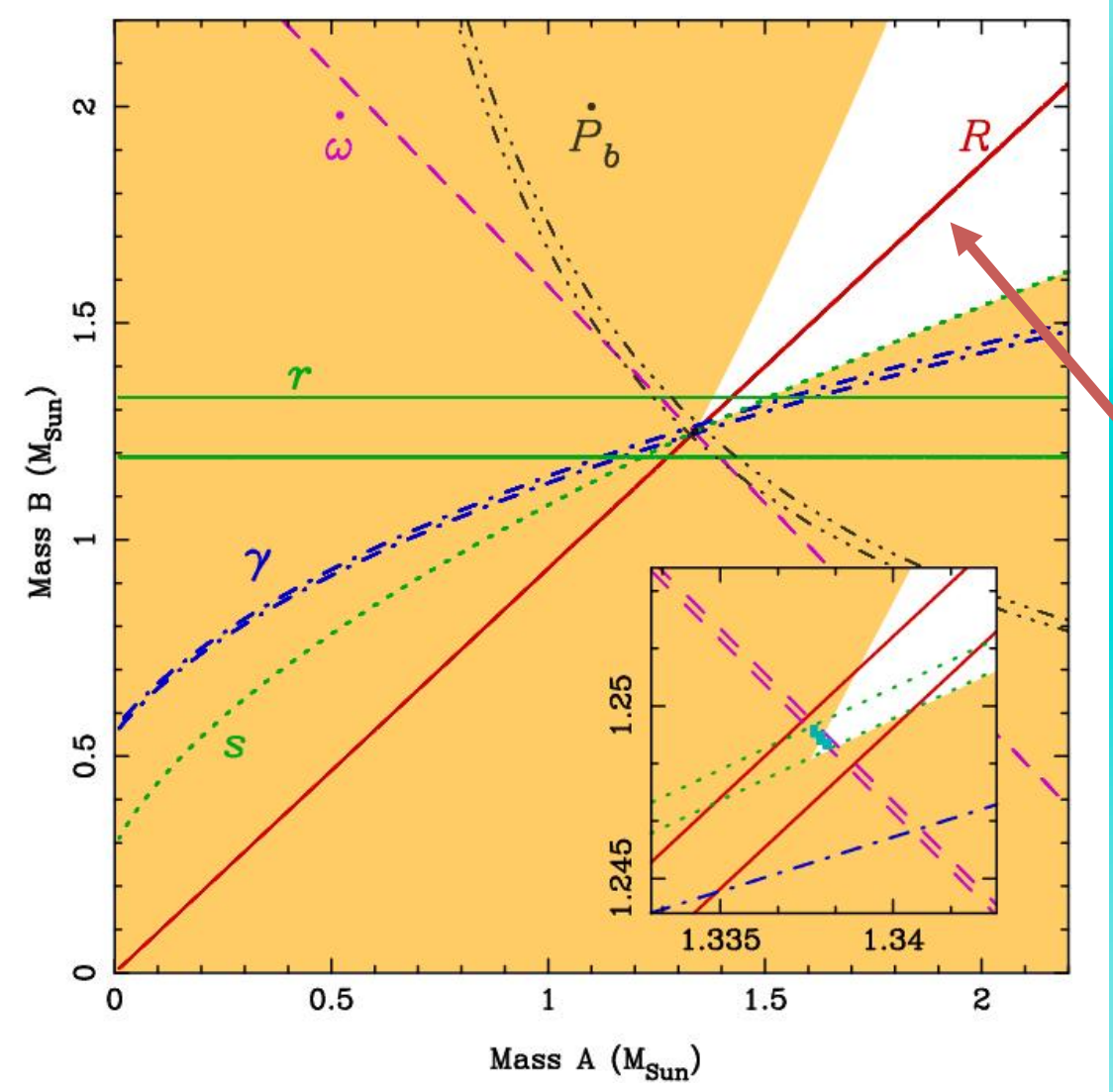


Kramer et al., 2006, Science **314**, 97.

Mass-mass diagram for the double pulsar J0737-3039A and B. In addition to 5 PK parameters (for A), we measure the mass ratio R. This is independent of gravitational theory ⇒ whole new constraint on gravity compared to other double-NS systems.

.

# Constraining Generic Theories with Multiple Pulsars

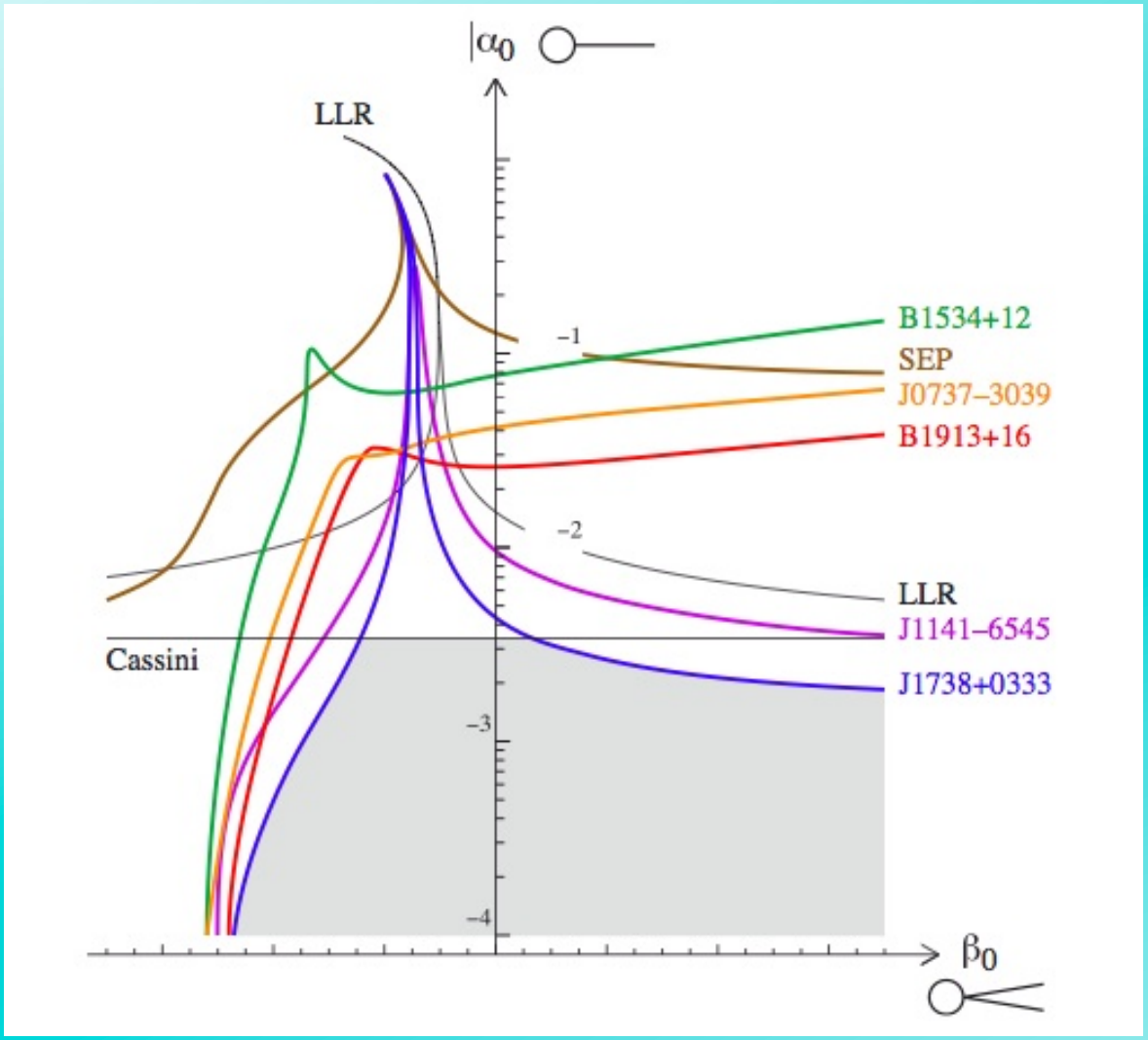


Strong constraints on parameters in alternate theories can be achieved by combining information from multiple pulsars plus solar-system tests (Damour & Esposito-Farese, Wex).

Freire et al. 2012, MNRAS **433**, 3328 for generic tensor-scalar theories of Damour & Esposito-Farese.

# Constraining Generic Theories with Multiple Pulsars

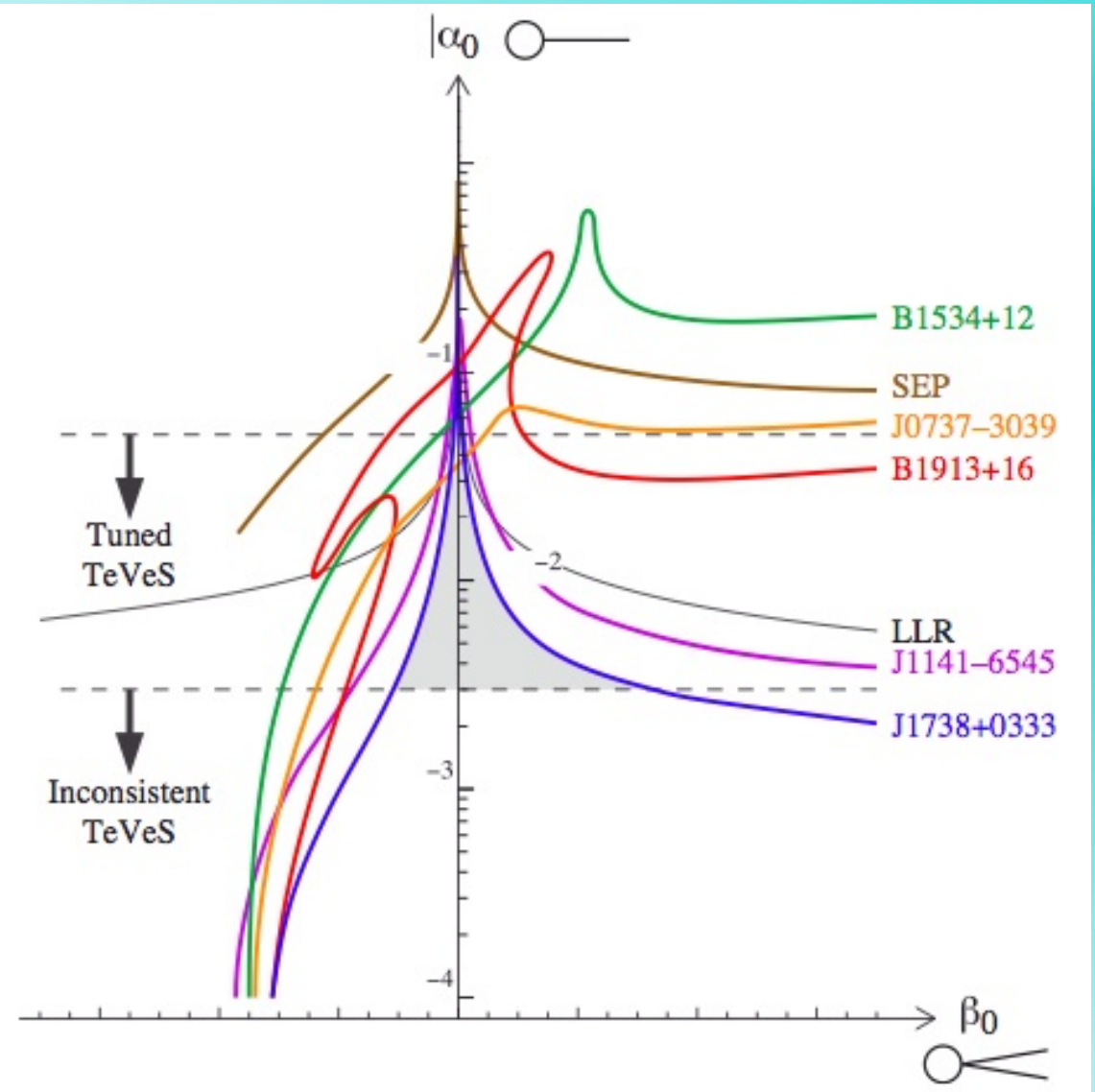


Freire et al. 2012, MNRAS **433**, 3328 for generalized TeVeS theories.

# Geodetic Precession

Before the second supernova:
all AM vectors aligned.

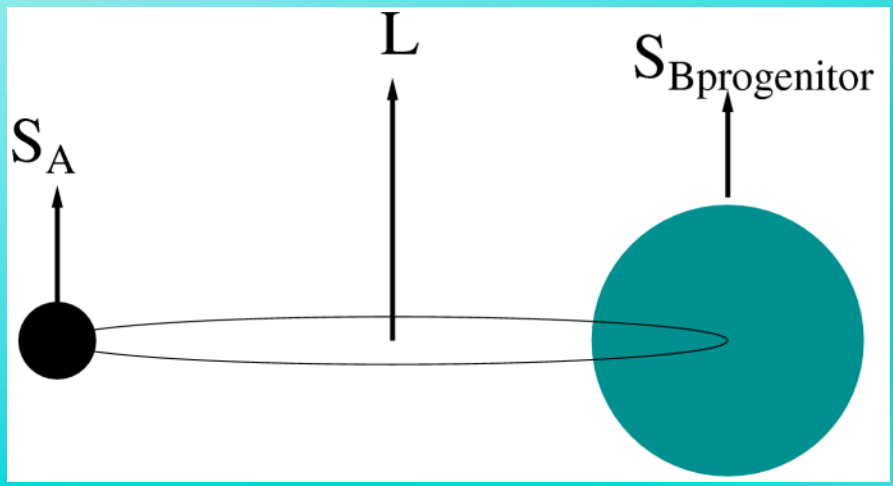


After second supernova: orbit tilted, misalignment angle δ (shown for recycled A); B spin pointed elsewhere (defined by kick?). Expect both spins to precess.

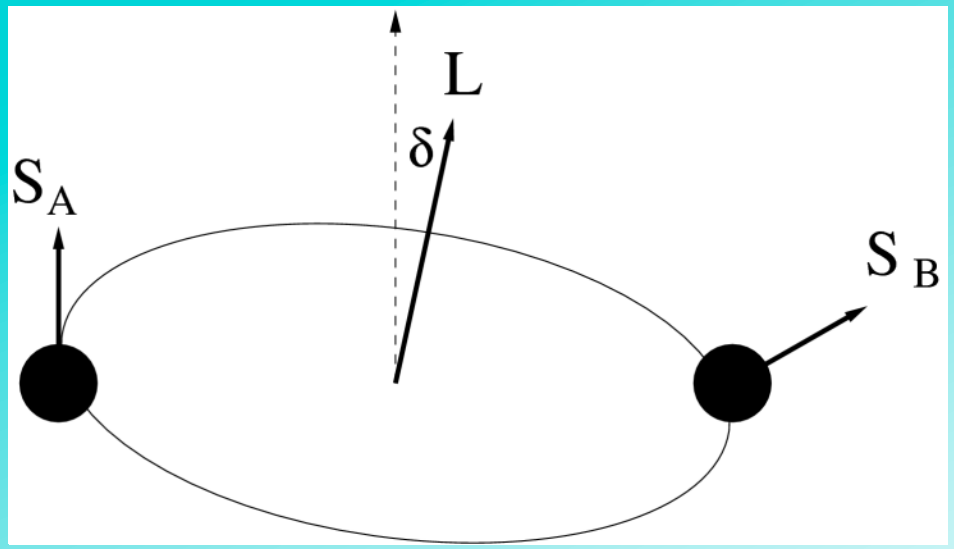

# Geodetic Precession

Precession period: 300 years for B1913+16, 700 years for B1534+12, 265 years for J1141-6545, 160 years for J1906+0746 and only ~70 years for the J0737-3039 pulsars.

It's seen in all of these (and now B2127+11C) except for the recycled pulsar 0737A.
This puts a limit on its misalignment angle of 3.2°, assuming two-pole emission (Ferdman et al. 2013, ApJ **767**, 85), implying little asymmetry in the supernova that formed B.

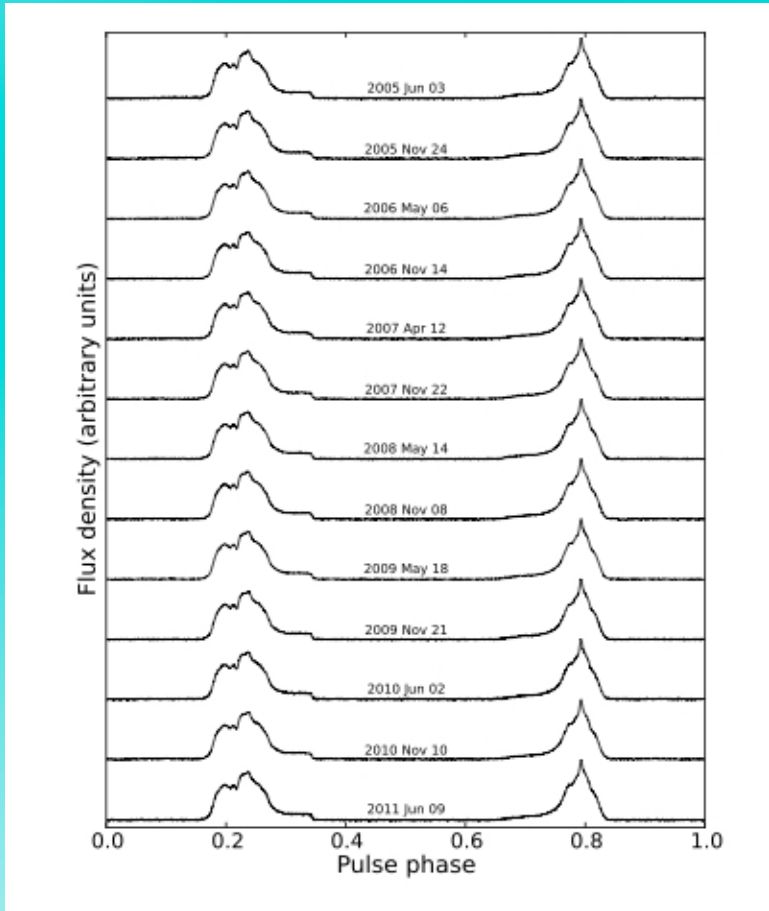

# PSR B1534+12 – Fonseca, Stairs & Thorsett 2014

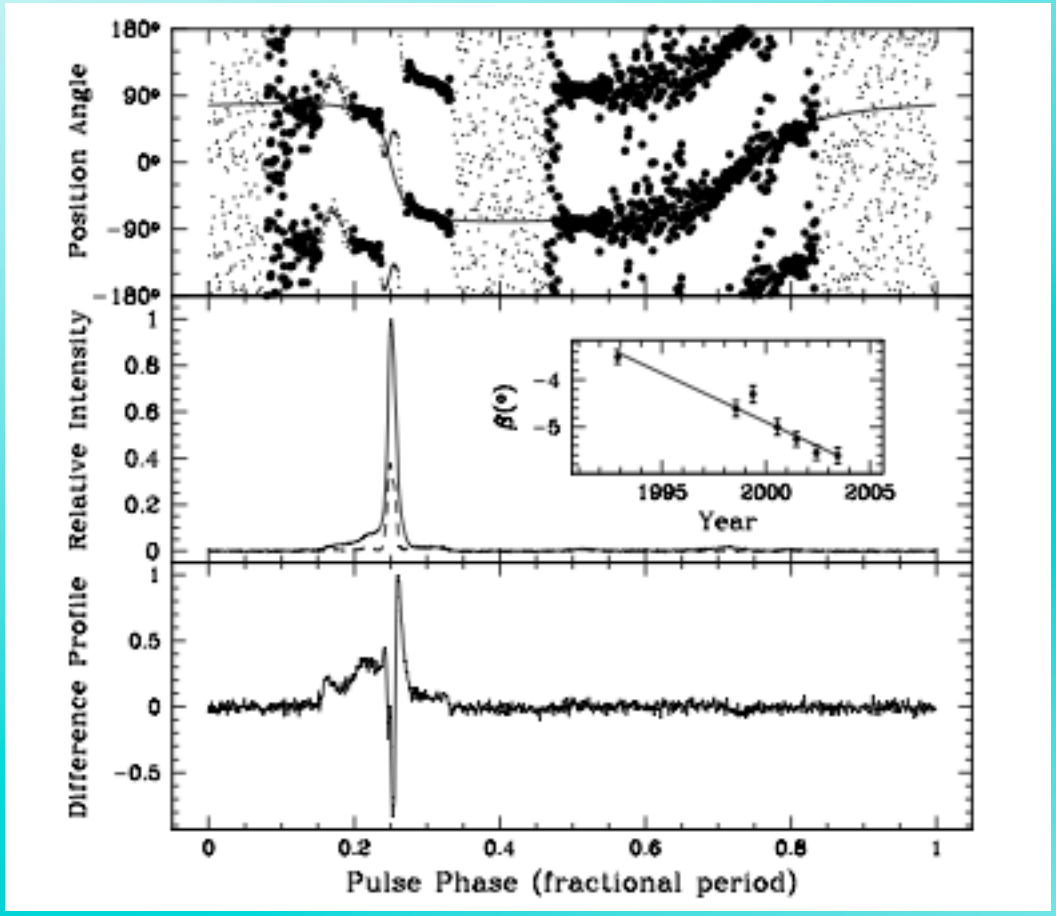


Stairs, Thorsett & Arzoumanian 2004

Long-term profile changes were identified by Arzoumanian (1995) and Stairs, Thorsett & Arzoumanian (2004). These continue into the ASP instrumentation era, although the 8-bit sampling of ASP meant that the profile looks a little different from the Mark IV profile.

(PUPPI data now being reduced!)

PSR B1534+12 – Measure precession by comparison to aberration.

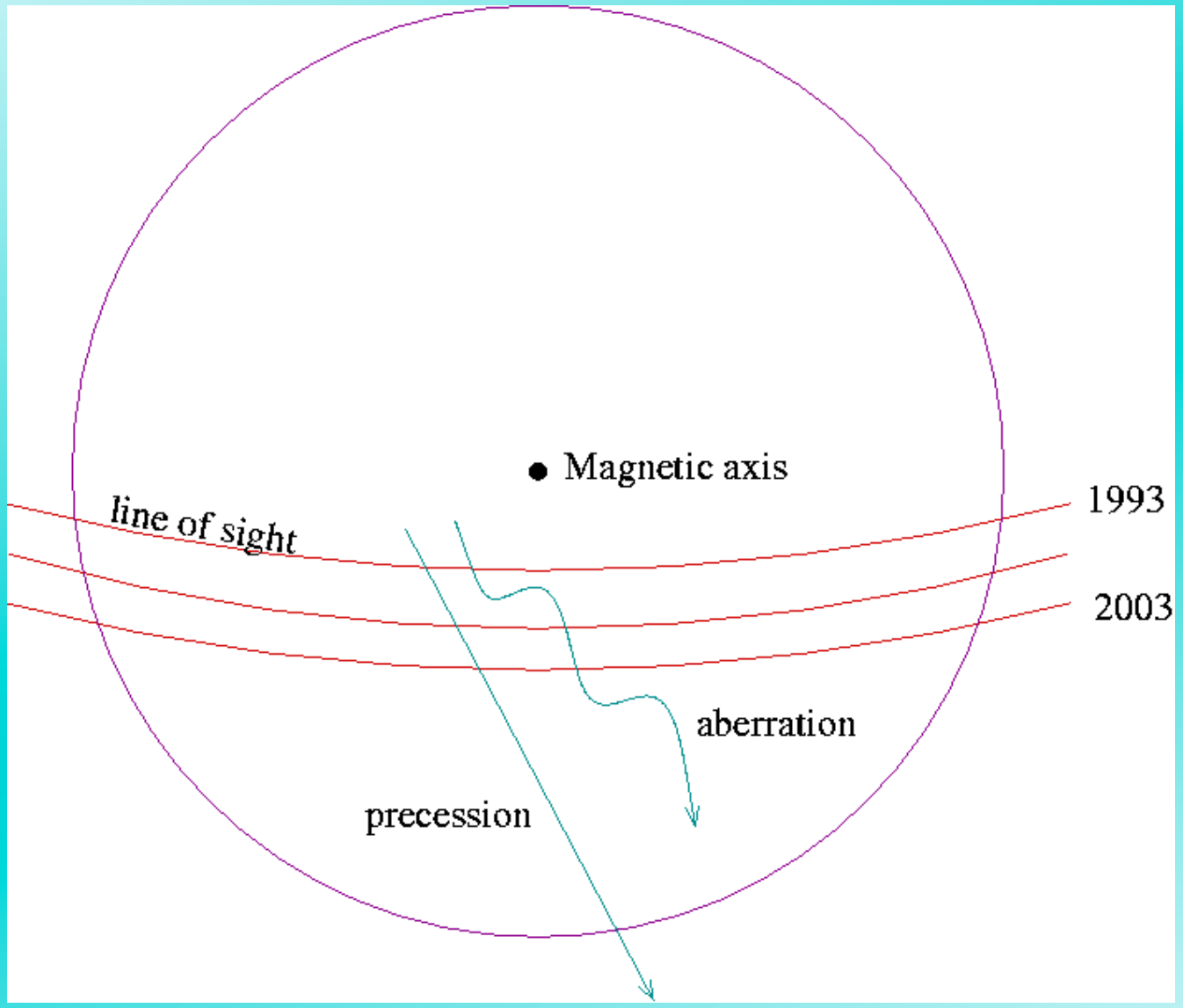


For long geodetic precession periods, the profile change should be ~linear over time, and the aberration (for the right geometry) should appear as a small fraction of the precession, with a periodic signal. Stairs, Thorsett & Arzoumanian (2004).

# PSR B1534+12 – Fonseca, Stairs & Thorsett 2014

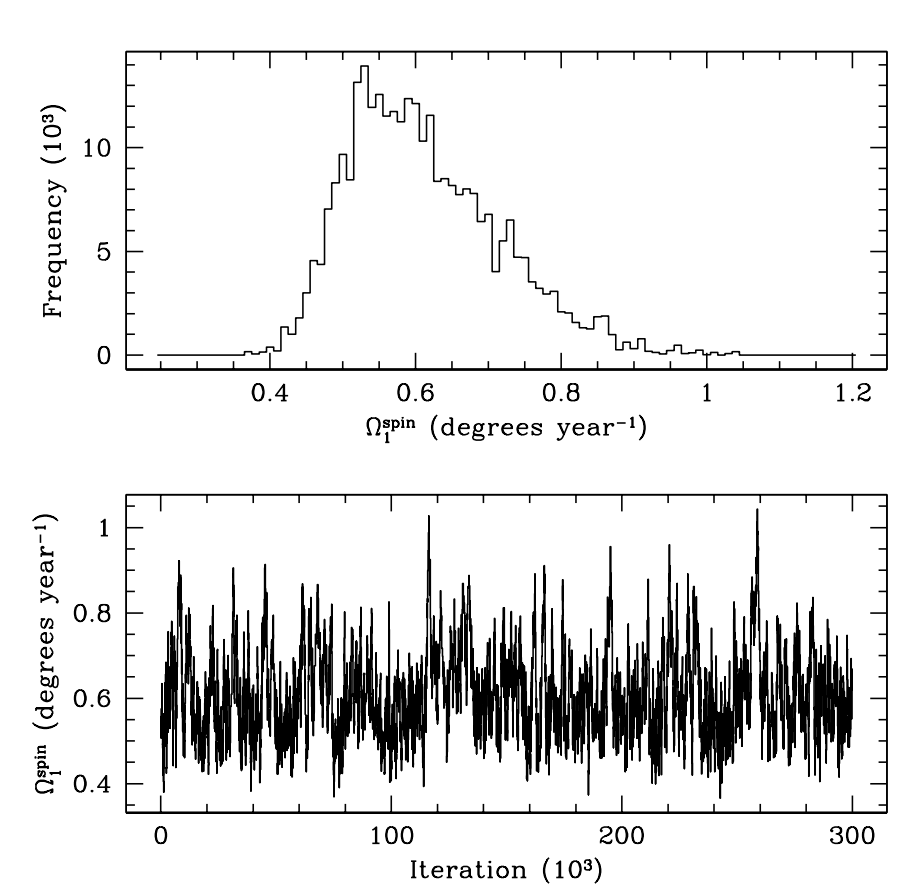


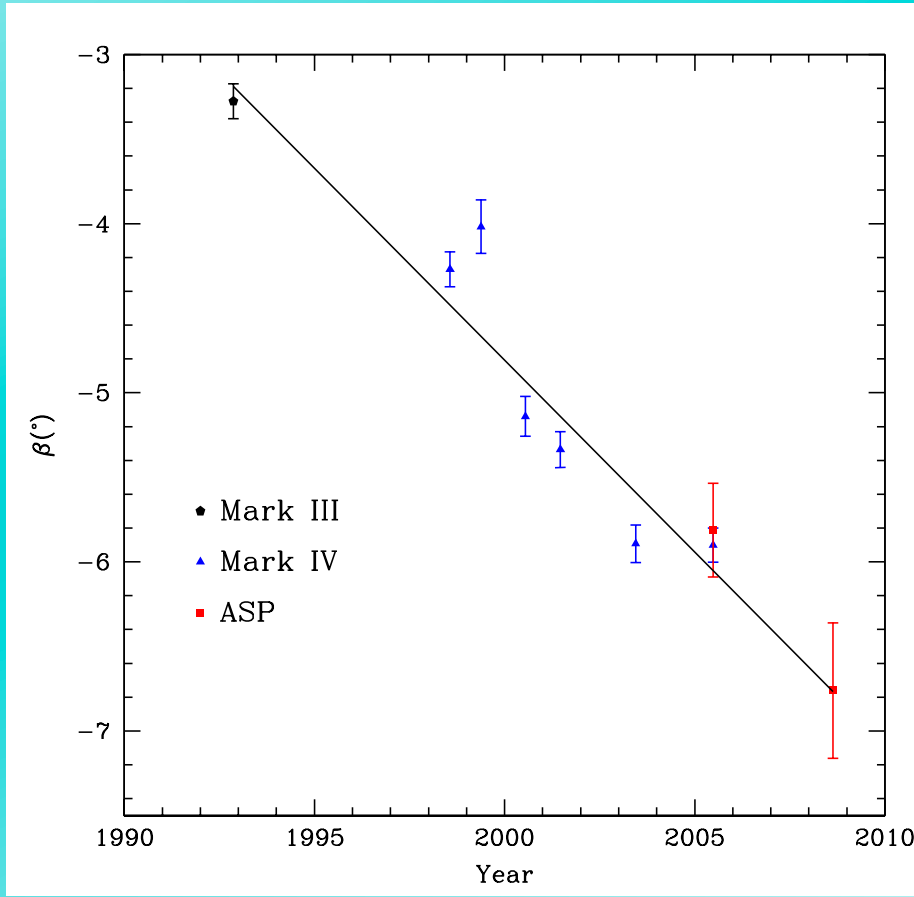


The rate of geodetic precession (via aberration) plus the slope of the long-term profile changes can be fit together via MCMC – and yield a precession rate consistent with the predictions of GR. This confirms and extends the analysis done in Stairs et al 2004. With the long-term changes in the RVM, we have the full geometry of the system; the spin-orbit misalignment angle is 27(3)°.

Meanwhile, in the double pulsar, B changed a lot....
and disappeared completely!

Dec. 2003

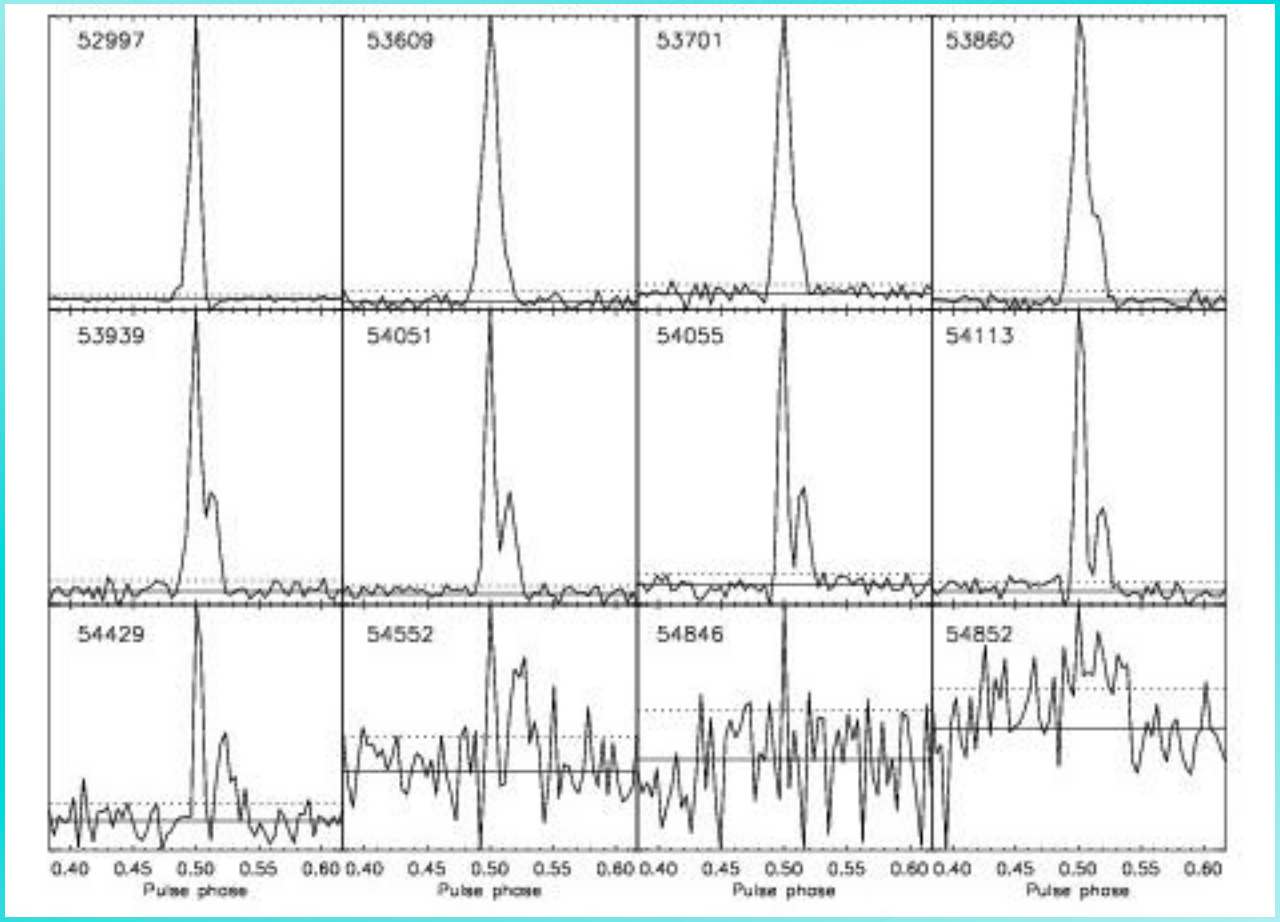


Jan. 2009

Perera et al., 2010, ApJ **721**, 1193

B's effects on A provide another avenue to precession:

Eclipses of A by B occur every orbit (Lyne et al. 2004, Science **303**,1153; Kaspi et al. 2004, ApJ **613**, 137). A's flux is modulated by the dipolar emission from B.

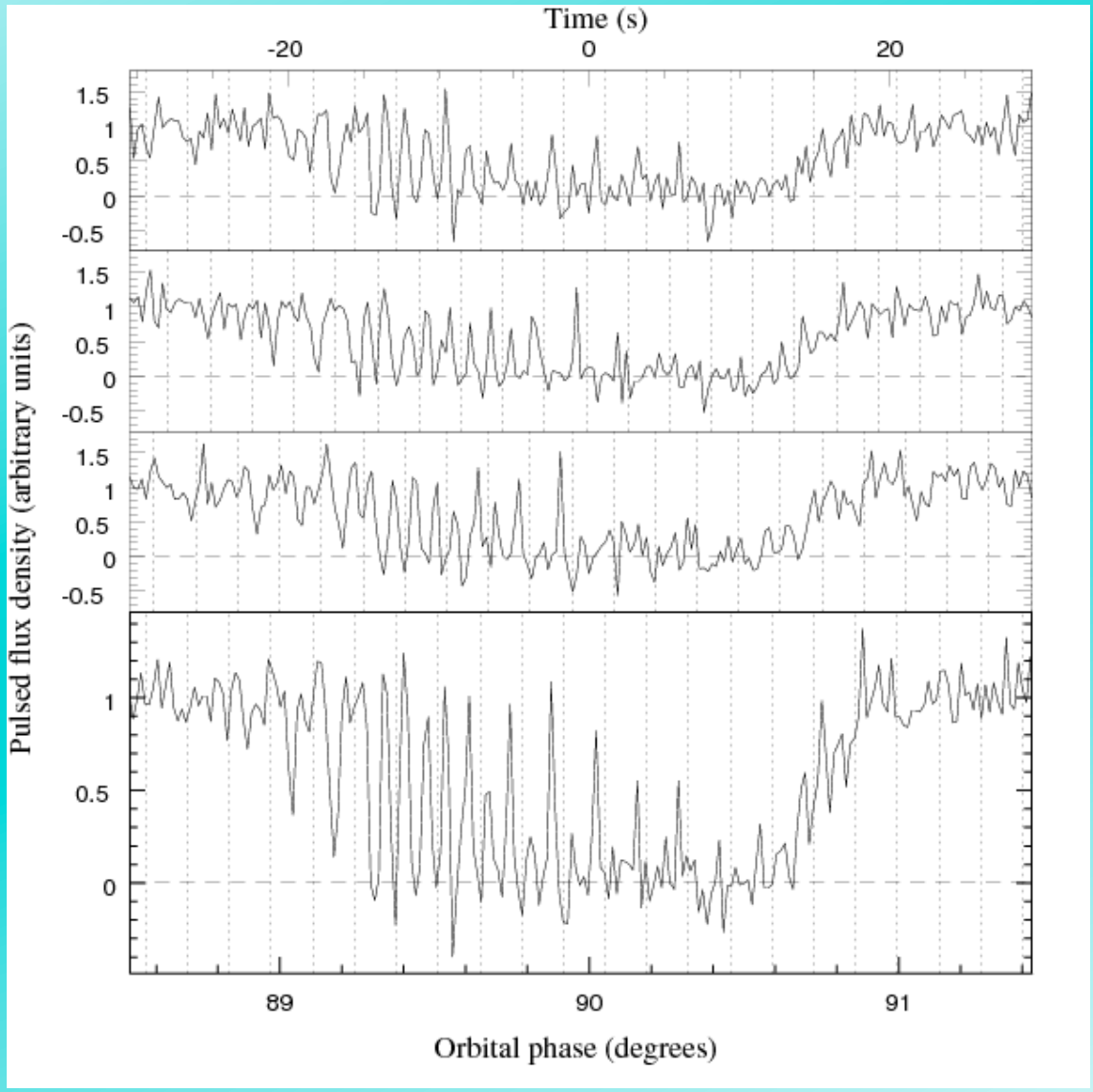


McLaughlin et al. 2004, ApJ **616**, 131

See Lyutikov & Thompson 2005 for a simple geometrical model, illustrated here for April 2007 data by Breton et al. 2008.

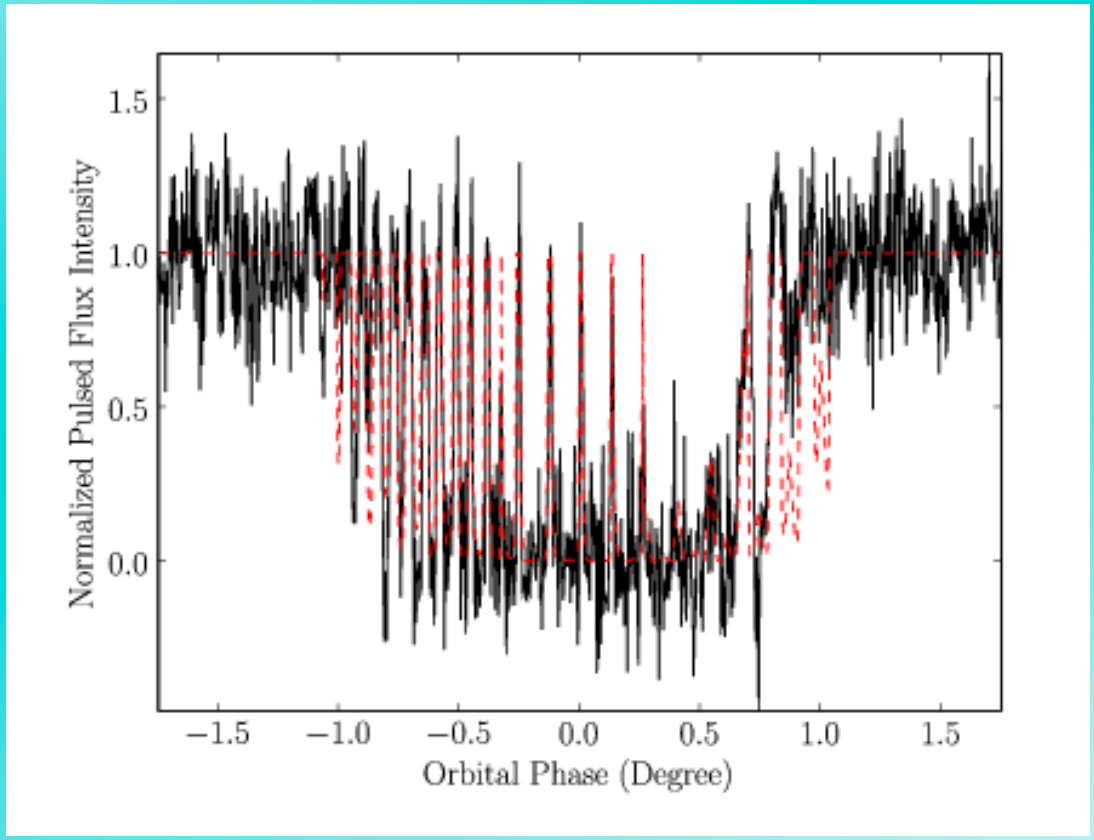

# Relativistic Spin Precession in the Double Pulsar

See Breton et al. (Science, 2008)

## Movie Description

The eclipses in the double pulsar PSR J0737-3039A/B occur when pulsar A's projected orbital motion, represented by a gray circle moving on a black line, passes behind its companion, pulsar B. Radio emission from pulsar A is absorbed via synchrotron resonance with the plasma trapped in the closed field lines of the truncated dipolar magnetosphere of pulsar B, shown as a colored dipolar structure. Since pulsar B's magnetic dipole axis is misaligned with respect to its spin axis (represented by a diagonal rod), the optical depth along our sight line to pulsar A varies as a function of pulsar B's spin phase. The theoretical light curve resulting from the eclipse animated in the upper panel is drawn as a black curve in the bottom panel and real eclipse data, observed with the Green Bank Telescope in April 2007, are overlaid in red. The animation speed corresponds to real time and the audio track is the sound that one would hear if the radio signal detected from pulsar A by the radio telescope was noise-filtered and amplified into an audio device. While individual pulsations from pulsar A are too fast to be distinguished, we can hear a mixture of F musical tones harmonically related to 44 Hz (F1 tone), the spin frequency of the pulsar, which is modulated in intensity as a result of the eclipse.

René Breton

See Lyutikov & Thompson 2005, ApJ **634**, 1223 for a simple geometrical model, illustrated here for April 2007 data by Breton et al. 2008, Science **321**, 104.

This model makes concrete predictions if B precesses...

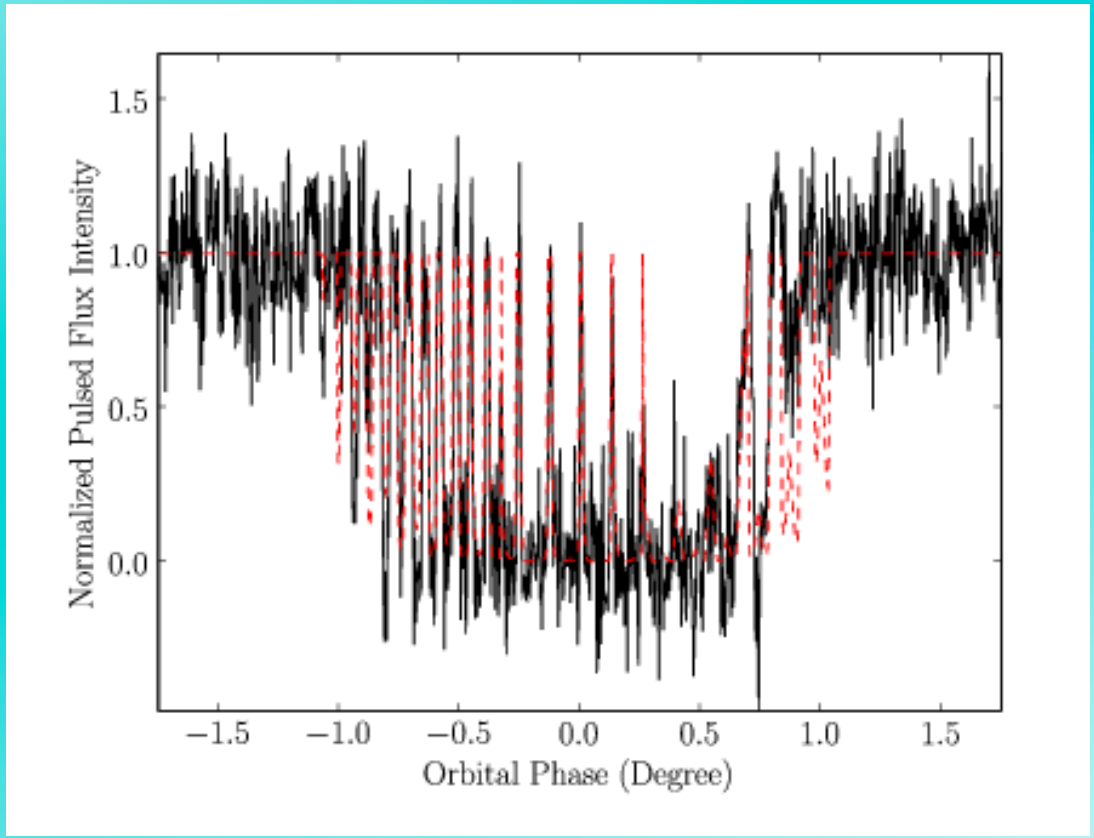

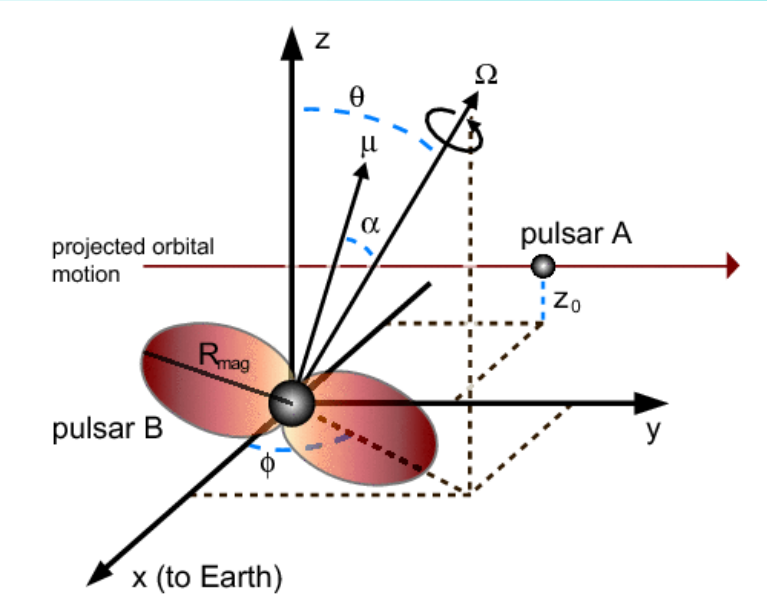


Eclipse geometry, Breton et al 2008. If B precesses, φ will change with time, and the structure of the eclipse modulation should also change... and it does!

Dec. 2003

Nov. 2007

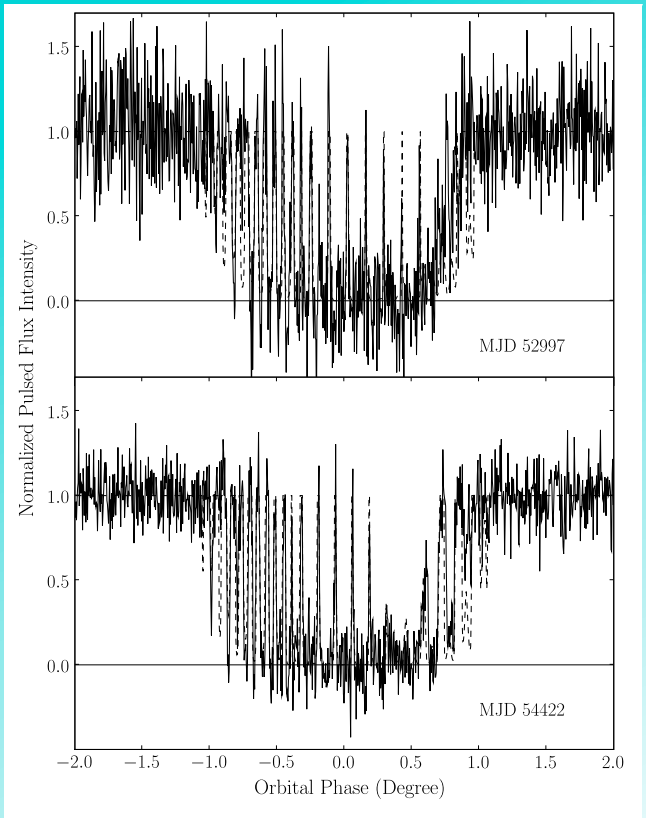


Courtesy René Breton

The angles $\alpha$ and $\theta$ stay constant, but $\varphi$ changes at a rate of $4.77^{+0.66}_{-0.65}$ $^{o}$ yr$^{-1}$. This is nicely consistent with the rate predicted by GR: 5.0734(7) $^{o}$ yr$^{-1}$.

And because we measure both orbital semi-major axes, this actually constrains a generalized set of gravitational strong-field theories for the first time!

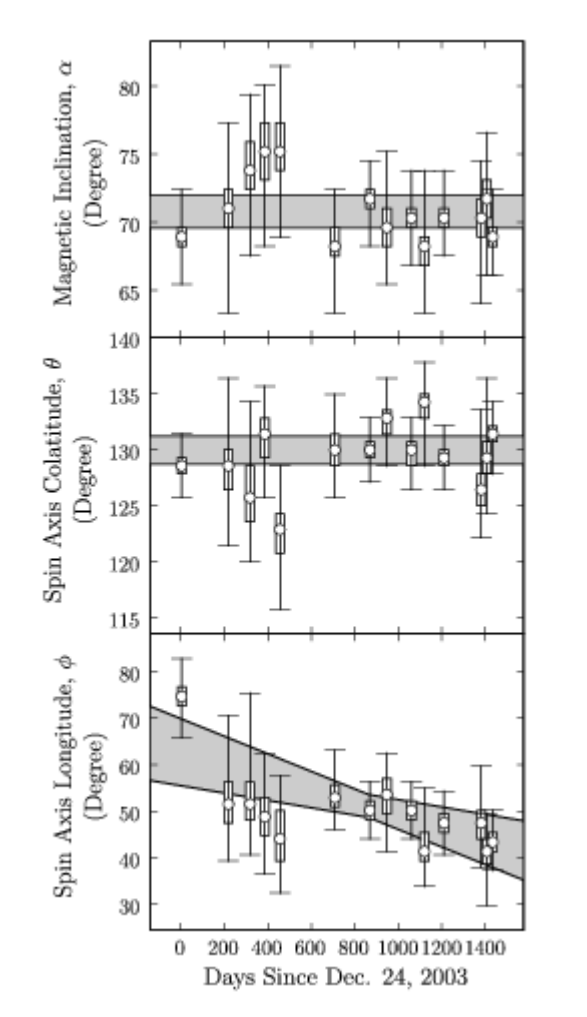


Breton et al 2008

**Chasing a direct detection of gravitational waves with pulsars**: 3 major collaborations.




Umbrella organization: the International Pulsar Timing Array
http://www.ipta4gw.org

Metric that includes a gravitation wave:

$$g_{\mu\nu} = \eta_{\mu\nu} + h_{\mu\nu}$$

This induces a Doppler shift in the pulsar signal:

$$\frac{\delta\nu}{\nu} = -\mathcal{H}_{ij}\left[h_{ij}(t_e, x_e^i) - h_{ij}(t_p, x_p^i)\right]$$

Strains at Earth and pulsar.

Geometric factor that depends on the angle between the Earth, pulsar and gravitational-wave source.

And therefore causes the pulsar timing residual to be:

$$R(t) = -\int_0^t \frac{\delta\nu(t)}{\nu} dt$$

(in addition to noise, systematics, etc.)

**Primary anticipated sources**: coalescing supermassive black-hole (SMBH) binaries, masses $10^6$ to $10^9$ $M_\odot$. Binaries are expected to form during galaxy mergers (eg Jaffe & Backer 2003) and with separations of < 1 pc, GW emission should be the main type of energy loss.

Representative signal size for a source of mass M/(1+z) with orbital frequency *f* at distance $d_L$:

$$\Delta\tau \sim 10\,\mathrm{ns}\left(\frac{1\,\mathrm{Gpc}}{d_L}\right)\left(\frac{M}{10^9\,M_\odot}\right)^{5/3}\left(\frac{10^{-7}\,\mathrm{Hz}}{f}\right)^{1/3}$$

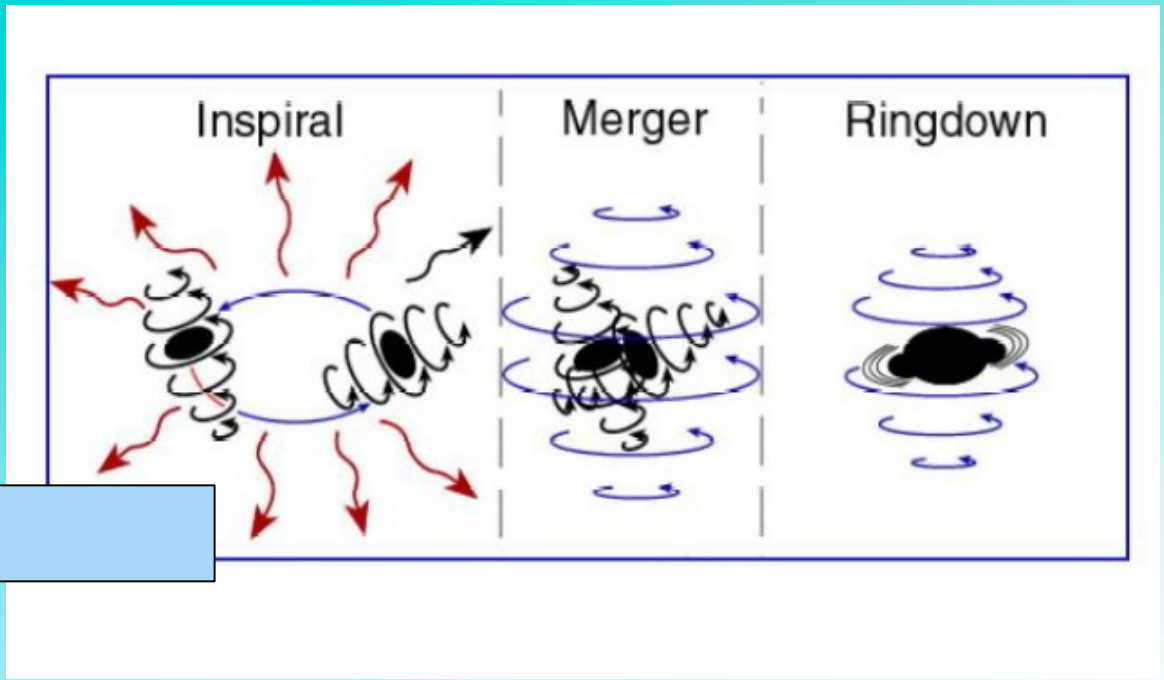


PTA Sources

Some recent simulations, showing expected sensitivities for the International Pulsar Timing Array now and in 5 years, relative to recent SMBH-binary models. The models vary depending on source-count modeling (whether from dark-matter simulations or using the observed properties of galaxies), relation of galaxy properties to SMBH mass and treatment of the astrophysics (eg eccentricity, stellar hardening, etc.).

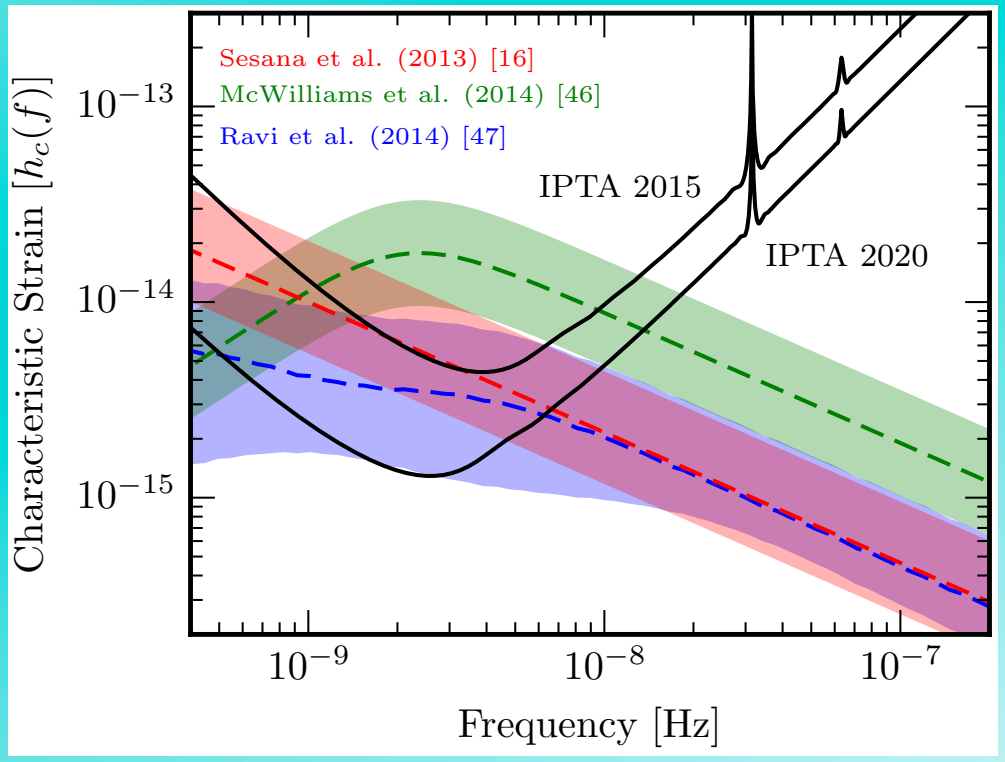

Recent limits from the various PTAs:

PPTA: Amplitude (at 1 year) < 1.0 x $10^{-15}$. This uses only 4 pulsars over 11 years, and at high frequency. Pure power-law models for the background aren't compatible with this limit. Shannon et al. 2015, Science **349**, 1522.

NANOGrav: Amplitude (at 1 year) < 1.5 x $10^{-15}$, using 18 pulsars over 9 years. Arzoumanian et al., ApJ, submitted.

EPTA: Amplitude (at 1 year) < 3.0 x $10^{-15}$, using 6 pulsars over 18 years. Lentati et al, 2015, MNRAS **453**, 2576.

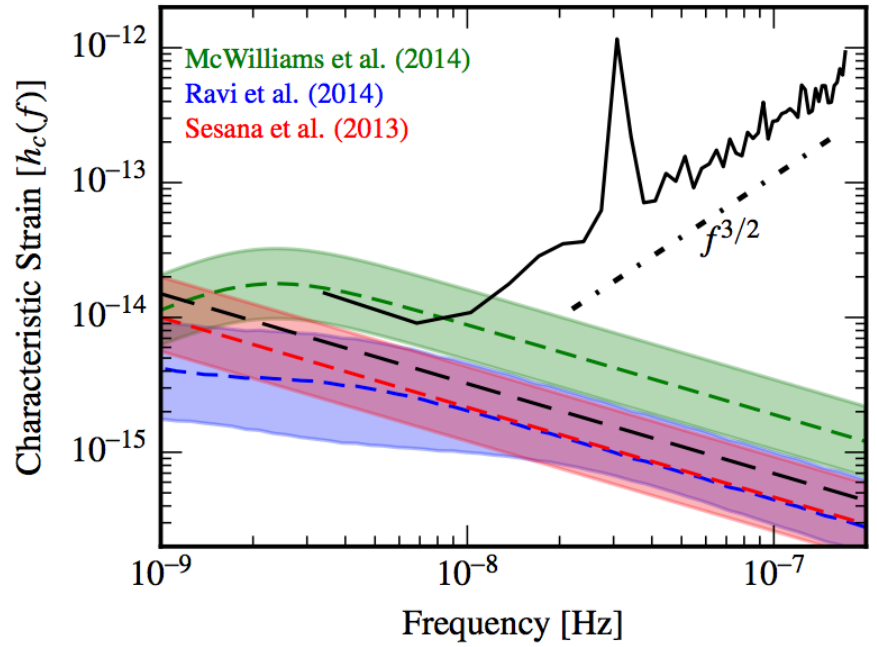


**Figure 2.** Strain amplitude vs. GW frequency. The solid black and long dashed black lines are the 95% upper limits from our spectral and power-law analyses. The red, blue and green shaded regions are the one-sigma predictions from the models of S13, RWS14, and MOP14. The green shaded region uses the simulation results from MOP14, but replaces the fit to the GWB predictions used in that paper with the functional form given by Eq. (24).

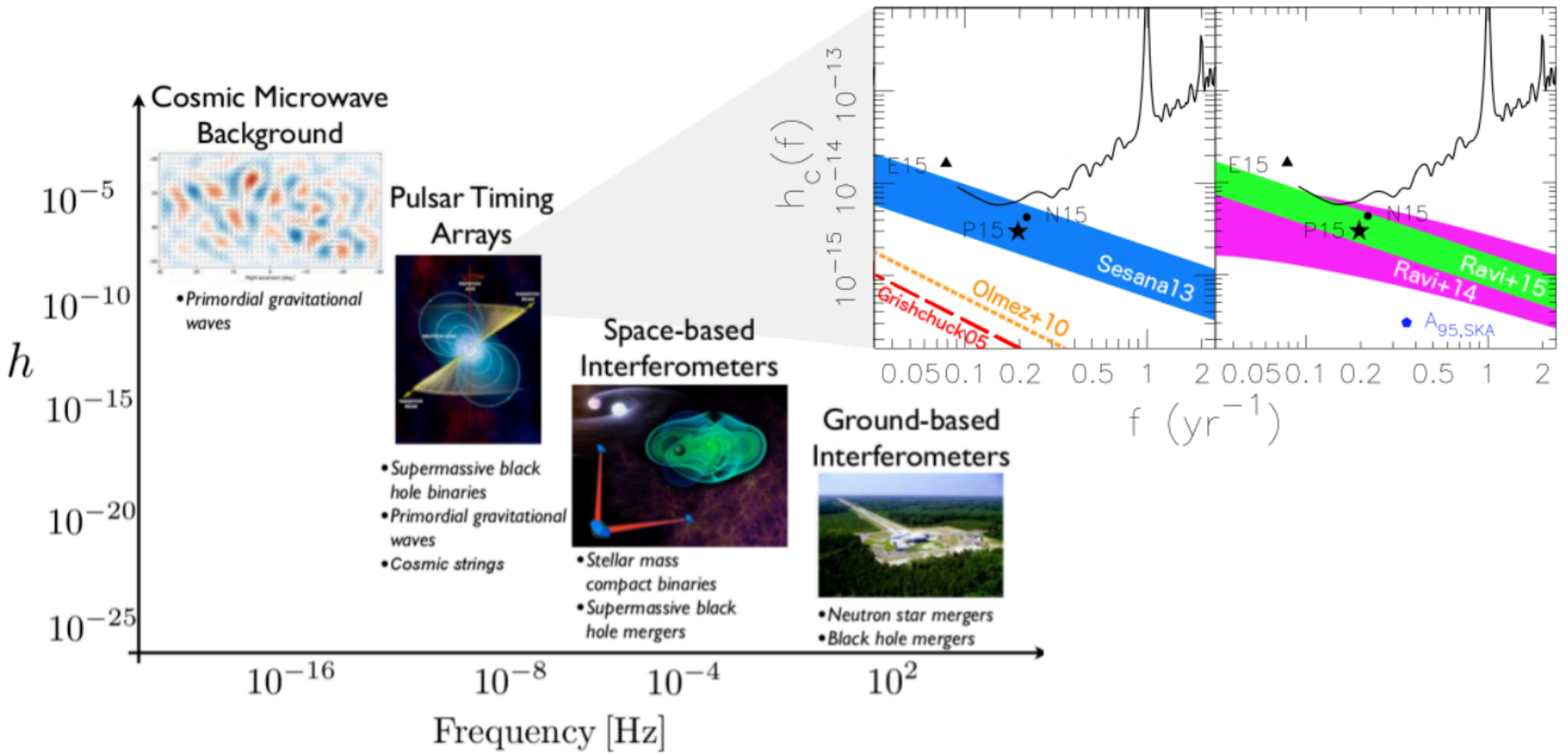


Fig. 1.— A conceptual strain spectrum, showing the complementarity of GW detection techniques adapted from a figure by NANOGrav. The anticipated sources, listed for each frequency range, are also complementary. The inset figure shows an enhanced view of the predicted GWB and limits in the PTA band (adapted and updated from Shannon et al. 2015). The 68% uncertainty range of several BSMBH simulations are indicated (filled curves), as are representative spectra from inflationary GWs (red long-dashed) and cosmic strings (orange short-dashed). The best limits are also shown; points are from PPTA, NANOGrav, and the EPTA (Shannon et al. 2015; Arzoumanian et al. 2015a; Lentati et al. 2015, respectively); the curve is from PPTA (Shannon et al. 2015).

Burke-Spolaor 2015, arXiv:1511.07869

# Future Prospects

Long-term timing of pulsar – white dwarf systems

$\Rightarrow$ better limits on $\dot{G}/G$ and dipolar gravitational radiation, as well as PPN-type parameters

$\Rightarrow$ better limits on gravitational-wave background from MSPs

Long-term timing of relativistic systems

$\Rightarrow$ improved tests of strong-field GR.

$\Rightarrow$ higher-order terms in $\dot{\omega}$ in 0737A and a measurement of its moment of inertia

Profile changes and eclipses in relativistic binaries

$\Rightarrow$ better tests of precession rates, geometry determinations.

Large-scale surveys, large new telescopes (CHIME, SKA)...

$\Rightarrow$ more systems of all types... and maybe some new "holy grails" such as a pulsar—black hole system...

See Shao, Stairs et al. on pulsar tests of GR with the SKA, arXiv:1501.00058